Geol. Mag. **154** (*2*), *2017, pp. 265–285.* © *Cambridge University Press 2016*
doi:10.1017/S0016756815001077

The Liuyuan Volcanic Belt in NW China revisited: evidence for Permian rifting associated with the assembly of continental blocks in the Central Asian Orogenic Belt

YU WANG*†, ZHAOHUA LUO*, M. SANTOSH*‡, SHUZHI WANG* & NA WANG*

*Institute of Earth Sciences, China University of Geosciences, Beijing 100083, China
‡Centre for Tectonics, Resources and Exploration, Department of Earth Sciences, University of Adelaide, SA 5005, Australia

(*Received* 20 September 2015; *accepted* 25 November 2015; *first published online* 3 February 2016)

Abstract – The basaltic pillow lavas in the Liuyuan region of NW China, considered to be part of an ophiolitic suite, have been central to the models on tectonic setting, evolution and timing of the final closure of the Palaeo-Asian Ocean. New field evidence on the sedimentary units associated with the basalts reveals comparable sequences in the northern and southern flanks of the Liuyuan Volcanic Belt with coarse to fine sediments from periphery to the centre. The dacites and rhyolites formed coevally with the pillow basalts. The pillow basalts are interlayered with lacustrine sandstone, claystone and clayey lake deposits. Detrital zircons from these sediments yield zircon U–Pb ages of 291–285 Ma. Andesites, dacites and rhyolites from the basaltic sequence yield U–Pb ages of 280–277 Ma, similar to the 282–280 Ma ages of gabbros that intrude the pillow lavas. All these rocks cover the 460–440 Ma granite and greenschist basement and have been intruded by gabbros of *c.* 272 Ma age, with subsequent (230–227 Ma) north–south contractional thrusting and folding. The data from our study are incompatible with the existing models that consider the basalts as part of an ophiolitic suite. Along the northern continental margin of China from west to east, the Tarim, Dunhuang-Alxa and North China cratonic areas all show evidence for regional extension through rifting during early–middle Permian time. These rift features and basaltic eruptions occurred coevally with the assembly of various microcontinental blocks against the Siberian craton at *c.* 300–250 Ma, synchronous with amalgamation of the Central Asian Orogenic Belt (CAOB) on the northern side of the Liuyuan Rift. These events were also broadly synchronous with formation of the global supercontinent Pangea.

Keywords: rift system, pillow-lava basalt, zircon geochronology, tectonics, Central Asian Orogenic Belt.

1. Introduction

Extensional tectonics, such as those along rifts within the interior and margins of continents and along spreading ridges in oceanic settings, have been a topic of global interest (e.g. Ziegler, 1992; Ziegler & Cloetingh, 2004; Sachau & Koehn, 2010; Liao & Gerya, 2015; Pirajno & Santosh, 2015). In continental areas, the origin of rifts and associated processes have been correlated to diverse geodynamics including disruption of supercontinents, orogenic lithospheric delamination and ascent of mantle plumes, among other models (Sachau & Koehn, 2010; Buiter & Torsvik, 2014; Nance, Murphy & Santosh, 2014; Pirajno, 2015; Wang *et al.* 2015). Major basaltic eruptions along the continental margins between an orogenic belt and continent have been attributed to post-orogenic eruptive activity, or related to a mantle plume. The tectonic setting or stresses that constrain volcanic eruptions during the period following oceanic subduction and collision and prior to intracontinental deformation is an important factor in evaluating the global significance of volcanic eruptions in continental interiors or along continental margins (e.g. Ziegler & Cloetingh, 2004). The process of convergence between plates involving the assembly of continents and microcontinents is complex; the contractional setting during this process can locally generate major rifts and volcanic eruptions which are different from those associated with regional extensional tectonics or through mantle plumes.

The Liuyuan Volcanic Belt is located within the Beishan region of NW China, which is connected to the NE extension of the Tarim Block and the Tianshan Orogenic Belt (Fig. 1). Previous studies have investigated the volcanic eruptions and tectonic setting of this belt and in adjacent regions (Li & Xu, 2004; J. B. Li *et al.* 2006; J. Y. Li *et al.* 2006; Xiao *et al.* 2009; Su *et al.* 2011*a*, *b*; Mao *et al.* 2012; Tian *et al.* 2013, 2014; Xu *et al.* 2014; Cleven *et al.* 2015), and also evaluated these with specific reference to the tectonics associated with the central Asian Orogenic Belt (CAOB) (Kröner *et al.* 2014; Safonova & Santosh, 2014), the largest Phanerozoic accretionary orogen around the world (e.g. Xiao & Santosh, 2014; Xiao, Sun & Santosh, 2015). The tectonic setting of the Liuyuan Volcanic Belt is debated, and it has been variously correlated with delamination

†Author for correspondence: wangy@cugb.edu.cn

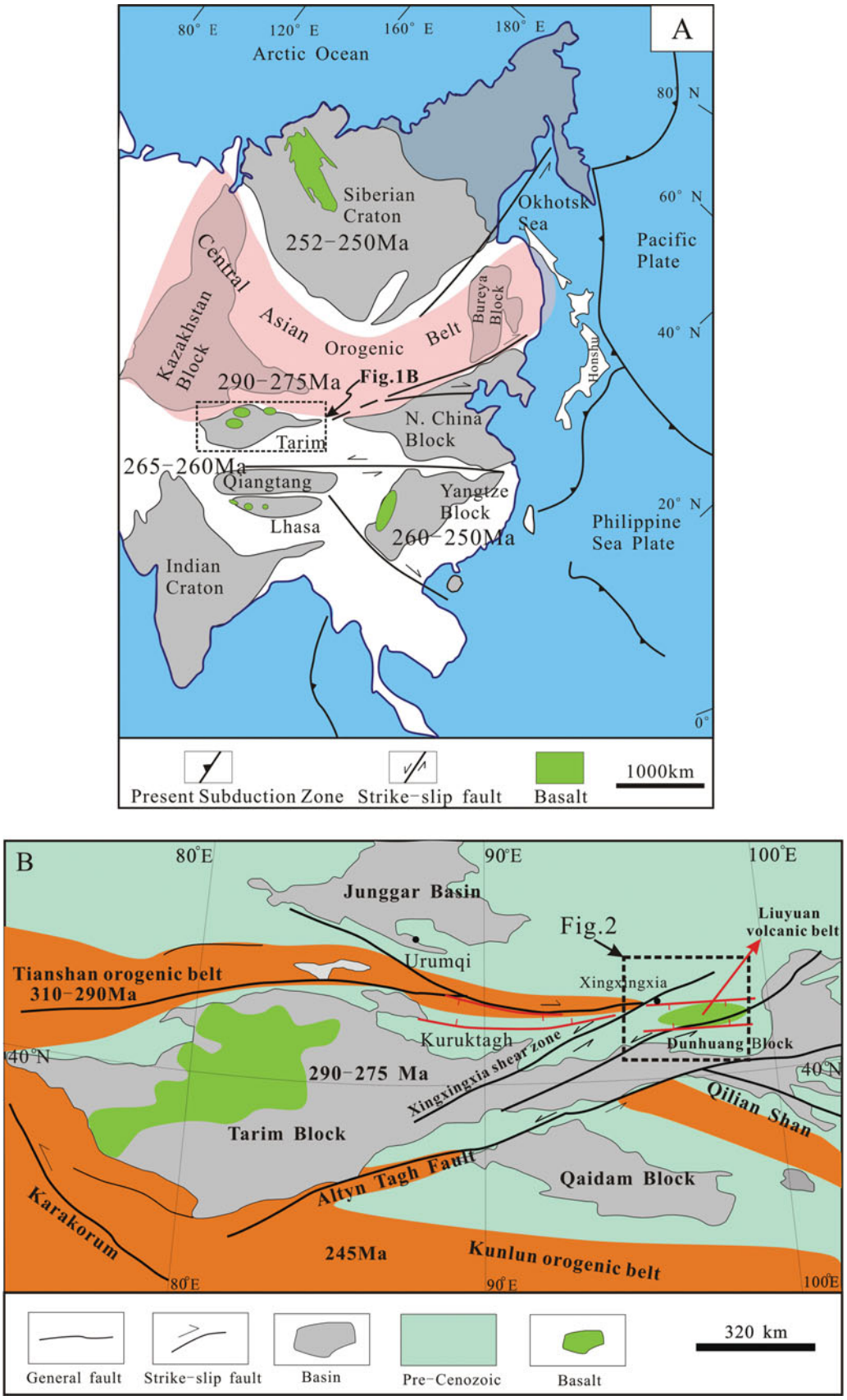

Figure 1. (Colour online) Tectonic setting of the Liuyuan Volcanic Belt and its adjacent regions. (a) 290–250 Ma basaltic eruptions, tectonic features and distribution of orogenic belts and continental blocks in Asia (from Wang *et al.* 2015). (b) Regional tectonic map of the Liuyuan Volcanic Belt and surroundings. The Tarim Block, Tianshan Orogenic Belt, Altyn Tagh Fault, Xingxingxia Shear Zone, the Dunhuang Block and the NE extension of the Tarim Block are shown.

https://doi.org/10.1017/S0016756815001077 Published online by Cambridge University Press

after the Tianshan Orogeny (Zhao *et al.* 2006), the Tarim mantle plume (Qin *et al.* 2011), a Permian–Triassic ophiolite complex (Xiao *et al.* 2009; Mao *et al.* 2012) and a rift system (Zuo *et al.* 1991; Zuo, Liu & Liu, 2003; Jiang *et al.* 2007). The geochemical data from the basalts have therefore been used to propose crustal delamination, related to the Tianshan Orogenic Belt after *c.* 320 Ma, and followed by collision and closure of the Palaeo-Asian Ocean (Han *et al.* 1998, 2011). On the basis of geochemical data and regional geology, Mao *et al.* (2012) and Xiao *et al.* (2009) concluded that the basaltic belt marks the southern margin of the CAOB (Altai region) and that it represents an ophiolite complex that marks the relic of the final closure of the Palaeo-Asian Ocean at *c.* 230 Ma. On the basis of 290–280 Ma basaltic eruptions in Tarim and eastern Tianshan, Qin *et al.* (2011) and many others have suggested that the basalts were the result of a mantle plume. Jiang *et al.* (2006, 2007) suggested that the volcanic rocks represent a rift system that formed after orogenesis in the CAOB, based on the petrology and geochemical features of mafic andesites and the magma generation correlated to re-melting of the continental lithosphere. Su *et al.* (2011*a*) marked the region as the 'Beishan Rift'. In all these arguments, the timing and tectonic setting of these events are vitally significant.

There are three main views regarding the tectonic setting of the formation of the Liuyuan Volcanic Belt. The first proposal is post-orogenic rifting or delamination of the lithosphere (Han *et al.* 1998) following the collision of the Tarim and Kazakhstan plates, which is proposed to have culminated before 300 Ma. This was followed by rifting and delamination with magmatism characterized by basaltic and related rocks through crust–mantle interactions. The second proposal is based on the idea that the basaltic pillow lavas belong to an ophiolite complex, and that they are related to the adjacent granites (460–400 Ma) and other Permian island-arc materials (Mao *et al.* 2012). These oceanic ridge materials are thought to have been involved in the final closure of the Palaeo-Asian Ocean, as late as 230 Ma (Mao *et al.* 2012). The basalt has also been correlated to a mantle plume (*c.* 280 Ma) (Zhou *et al.* 2004; Qin *et al.* 2011) that affected the entire western part of NW China during early Permian time.

The models above describe three contrasting tectonic settings: contraction (ophiolites in the zone of plate convergence), extension (delamination or rifting) or a mantle plume (ascending from depth). In terms of modern tectonics, four possible scenarios can be envisaged for the formation of a mantle plume such as rifting, spreading at an oceanic ridge and continental or orogenic delamination. This raises a number of questions, including the following. (1) Are the mid-oceanic-ridge-basalt- (MORB-) type basalts related to the opening of an ocean basin, a rift, delamination or an ocean-island-basalt (OIB-) type magmatic source? (2) What characterizes the sedimentary sequences and structural deformation associated with the basaltic rocks in the Liuyuan Volcanic Belt, between continental margin and continental interiors? (3) What is the relationship between gabbros and basalts in the region? Do the gabbros represent the closure of an ocean basin, a thrust system or are they just intrusive contacts? Where are the cherts from the oceanic realm? The lack of appropriate answers to these questions reflects the fact that field geology and other characteristics of the rocks remain unclear. Of relevance is the fact that similar basaltic systems have formed regionally and mainly along the northern margin of China, such as in association with the Tarim, Dunhuang-Alxa and North China blocks (Fig. 1B), as well as in the southern Kyrgyz Tienshan (Simonov *et al.* 2015). This observation is important in deducing the nature of the magmatic evolution and tectonic setting, but it remains unclear (1) whether or not such events are typical of a collision belt and (2) whether they are related to the post-collisional period or the assembly of continental blocks during the formation of the Pangea supercontinent. It is also important to evaluate, on the crustal or lithospheric level, whether the basaltic rocks represent extension or a rift developed in a collisional belt, and if the margin of the continental block has been overprinted.

In this paper, we present detailed cross-sections from field investigations, describe structural patterns, present results of microstructural analyses and discuss age constraints from zircon U–Pb geochronology. We also compare the tectonic setting of basaltic volcanic rocks along the continental margin of north China, such as in the Tarim, North China Craton, the Dunhuang-Alxa and microcontinental blocks, in an attempt to reconstruct the volcanic and related events that took place during the assembly of these continental blocks during Permian time. We also discuss the origins of the magmas, horizontal flow regimes and magma upwelling.

2. Tectonic setting and geological features

2.a. Tectonic setting

The Liuyuan Volcanic Belt is located on the corner of the NE extension of the Tarim Block (Figs 1b, 2). It is bounded by the Dunhuang-Alax Block (*c.* 900 Ma) to the south, and is connected with, and subparallel to, the Xingxingxia sinistral ductile shear zone on its NW side (Fig. 2). It is also connected to the Tianshan Orogenic Belt on its western side and the Inner Mongolia Orogenic Belt to the east, which is possibly the southern boundary of the CAOB (Xiao *et al.* 2010). On both the southern and northern sides of the volcanic belt the volcanic and associated sedimentary rocks cover a variety of older rocks, including Ordovician–Silurian metamorphic and magmatic rocks, and metamorphosed granites and granodiorites that may represent a late Permian – Mesozoic island arc (Mao *et al.* 2012). The sinistral Xingxingxia and Altyn Tagh faults cut the Liuyuan Volcanic Belt on the NW and SE sides, respectively. Regionally, the Liuyuan Volcanic Belt is situated between the Tarim and Dunhuang-Alxa blocks,

https://doi.org/10.1017/S0016756815001077 Published online by Cambridge University Press

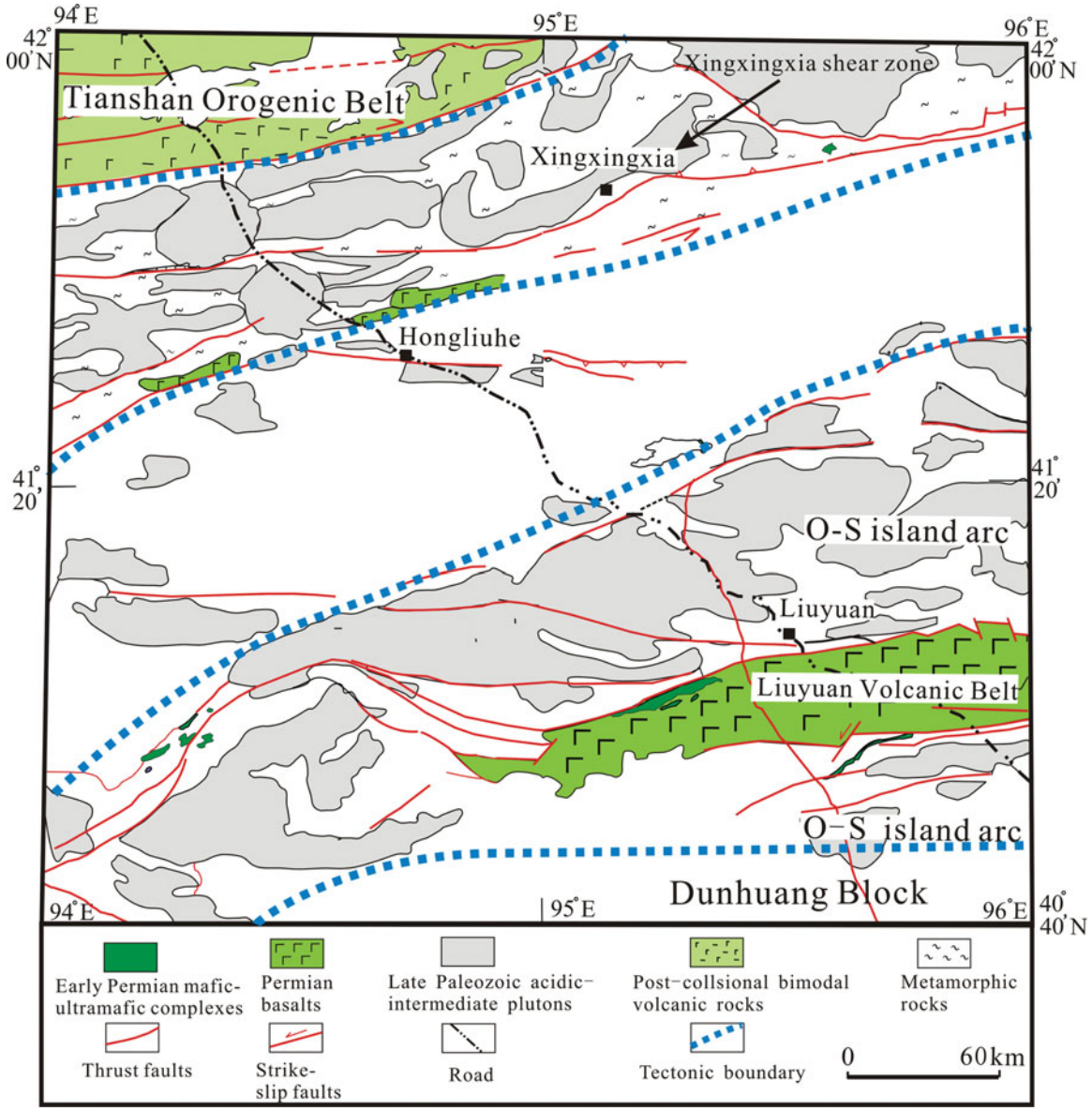

Figure 2. (Colour online) Tectonic features of the Liuyuan Volcanic Belt and the connected Tianshan Orogenic Belt and Dunhuang Block. O-S – Ordovician–Silurian.

and on the northern margin of the Dunhuang Block between the Siberian and Tarim–Qaidam blocks.

2.b. Sedimentary sequences and their characteristics

From north to south, the Liuyuan Volcanic Belt comprises Ordovician–Silurian granite/metamorphic rocks that are overlain by a series of coarse volcanic-bearing sandstones with thin conglomerates, coarse sandstones, sandstones, fine-grained sandstones, claystones and black shales (Figs 3–6). The central part of the region is composed of basaltic pillow lavas and volcanic conglomerates (Figs 3–4). In the south, running from south to north there are metamorphosed granites of Ordovician–Silurian age, claystones that have been affected by contact metamorphism, steeply dipping schists, fine-grained sandstones, sandstones, coarse-grained sandstones and sandstones containing small pebbles. The sedimentary sequences on the southern and northern sides of the volcanic belt are comparable in both lithology and age (Fig. 6).

The sedimentary sequence on the northern side of the Liuyuan Volcanic Belt is continuous and well exposed on the NW side of Liuyuan Town and in a valley in the far east of the area (Fig. 3). There are clasts of basalt, rhyolite and tuff within the coarse or pebbly material (Figs 4, 5). Underlying the pebbly material are fine-grained conglomerates and interbedded conglomerates and sandstones. Steeply dipping pebbly layers and tuffs occur in the sedimentary sequence, and the tuffs contain fragments of granite and schist (Fig. 5a, b). On the northern side of the belt, the coarse sedimentary rocks lie directly on top of Ordovician–Silurian schists and granite. Not only were fragments of granite and schist deposited together with the tuff, but we also found subaqueous slump structures in the sandstones. The coarser sedimentary rocks are overlain by black fine-grained sandstone and claystone, with a

https://doi.org/10.1017/S0016756815001077 Published online by Cambridge University Press

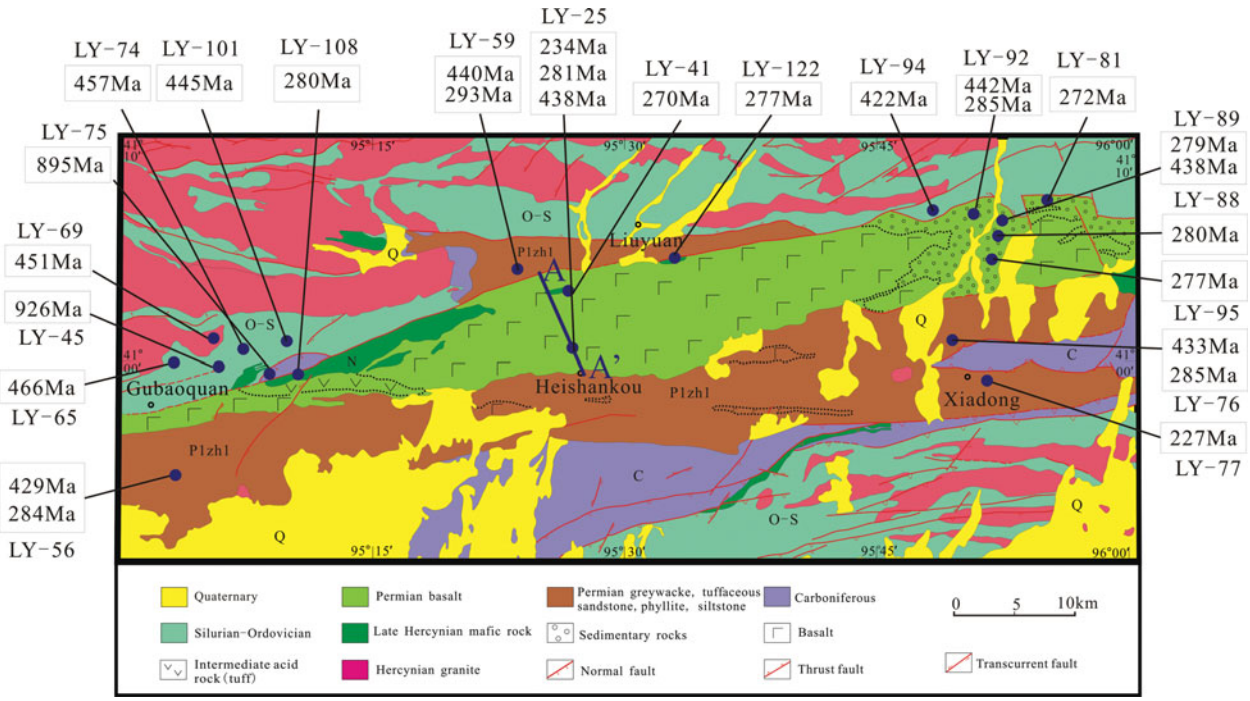

Figure 3. (Colour online) Geological map of the Liuyuan Volcanic Belt. Age data, sample locations and cross-section in Figure 4 are shown. Q – Quaternary; P1zh – Early Permian Zheshi Formation; C – Carboniferous; O-S – Ordovician–Silurian.

continuous sequence of subaqueous deposits. On the southern side of the belt we have observed contact metamorphism of claystones by the basalt, with a sharp contact between the basalt and hornfelsed claystone, clearly showing that the black sandstones and claystones were deposited before the eruption of the basalt. Along the central part of the volcanic belt within the pillow lavas are soft claystones that contain pebbles of basalt, which shows the basalt was erupted in a lake or deep water. There are also some conglomerates with rhyolite clasts.

Late Permian – Middle Triassic reddish volcaniclastic sandstones are common. Synsedimentary volcanic eruptions are also evident where basaltic, rhyolitic and dacitic material was directly incorporated into the muds and clays on the lake floor. However, there are no cherts, limestones or dolomites associated with these volcanic rocks.

2.c. Structural features

A variety of structures have affected the Liuyuan Volcanic Belt, such as ENE–WSW-trending strike-slip faults, vertical thrust faults and inclined folds. Overall, the region is characterized by a series of synclines that fold the layers of sediment and volcanic material (Figs 5g, h, 7). The layers dip to the south on the northern side of the belt and, south of the pillow-lava basalts, dip to the north. On the southern side of the belt, a recumbent fold that verges southwards is associated with thrust faulting (Fig. 5h). In the central part of the basaltic belt, a large amount of WSW–ENE-aligned strike-slip motion has affected the tuff and basalt layers (Fig. 5g). Basalts inclined at a high angle form drag folds within the strike-slip fault zone, but not elsewhere. On the northern side of the belt, although the sedimentary sequence dips to the south, north-dipping thrust faults are exposed along the boundary between the sediments and the basalts. These thrust faults cut through the gabbro, schist and dacite, suggesting that the faulting postdates all those rocks. Within the basaltic belt folding has resulted in the rocks dipping both north and south, generating complex folds although no thrust fault as reported in the cross-section of Mao *et al.* (2012) was identified. Close to where the basalts were erupted, the fine-grained and black-coloured sandstones show steep dips. A summary of the kinematics of the region is provided in Figure 7, clearly revealing the north–south-aligned compression that is expressed generally as a transpression.

A mylonite-bearing ductile shear zone was identified on the northern side of the belt, although the shear zone only affects the Ordovician–Silurian greenschists and does not represent a sheared boundary between the Ordovician–Silurian rocks and the Permian sedimentary sequences. The granites and the Ordovician–Silurian metamorphic rocks have been thrust over the gabbros and basalts of the Liuyuan Volcanic Belt, but only brittle deformation is observed along that thrust.

2.d. Volcanic profiles and their features

The basaltic pillow lavas are commonly weathered and eroded, carbonatized and chloritized, and have been variably folded. Volcaniclastic rocks with both felsic and mafic fragments are observed within the basaltic layers. Between the layers of pillow lava there are sandstones, claystones and mud-carbonate sandstones

https://doi.org/10.1017/S0016756815001077 Published online by Cambridge University Press

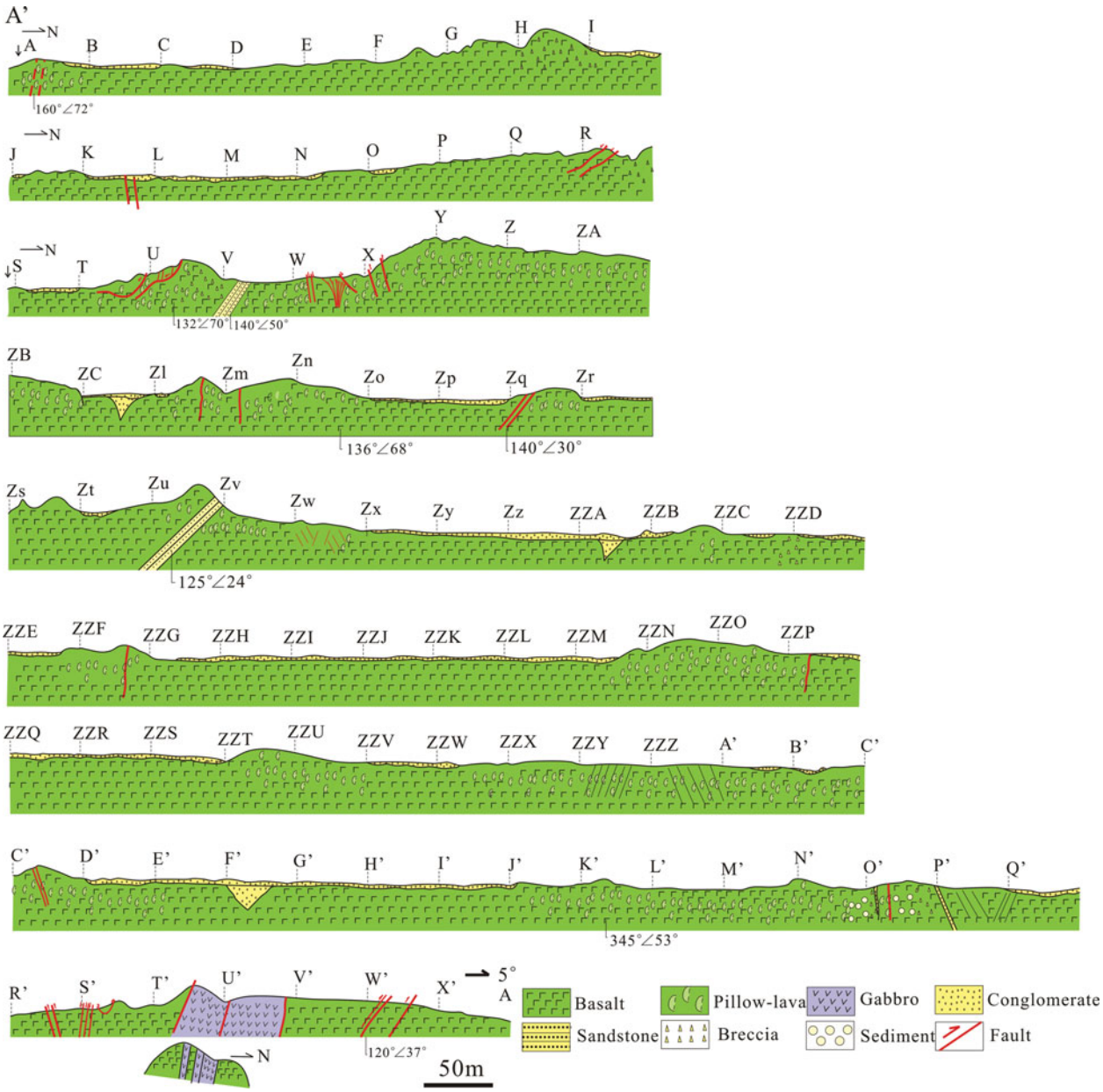

Figure 4. (Colour online) Cross-sections of the Liuyuan Volcanic Belt. Cross section A–A' is indicated in Figure 3.

(described as chert by Mao *et al.* 2012; Figs 4, 5c, d), and it is evident that claystones were being deposited in the lakes at the same time that the basalts were erupted. The pillow lavas are found in the central part of the volcanic belt, but on both the northern and southern sides of the belt there are no pillow lavas. In the extreme NE part of the basalt domain, claystones and other fine-grained sediments occur with layers that contain rhyolitic and andesitic material. The volcanic rocks are not only basalt, but also include felsic, intermediate and mafic magmatic units (although not necessarily together in the same area). Detailed cross-sections across the Liuyuan Volcanic Belt are shown in Figures 4 and 6b. Within the pillow lavas there are claystones, but no fossils have been found. The basaltic rocks (which have trachytic textures) and the accompanying rhyolites and dacites have been described by Jiang *et al.* (2006).

2.e. Magmatic features and ages of the intrusions: constraints on the timing of tectonic events

On both the northern and southern sides of the basaltic pillow lava are vast exposures of granite and schist of Ordovician and Silurian age (see the following section for the results of zircon LA-ICP-MS dating). Giant mafic dykes that run parallel to the main east–west-trending structural lines of the area also occur. The dykes formed earlier than the main pillow basalt eruptions.

Regardless of their coarse- or fine-grained nature, the gabbros and olivine gabbros display intrusive relationships with the eruptive basaltic rocks (Fig. 5e, f) and the contacts between gabbro and basalt are not thrust faults. Examples are found at Gubaoquan and other places where coarse- and fine-grained gabbros have

https://doi.org/10.1017/S0016756815001077 Published online by Cambridge University Press

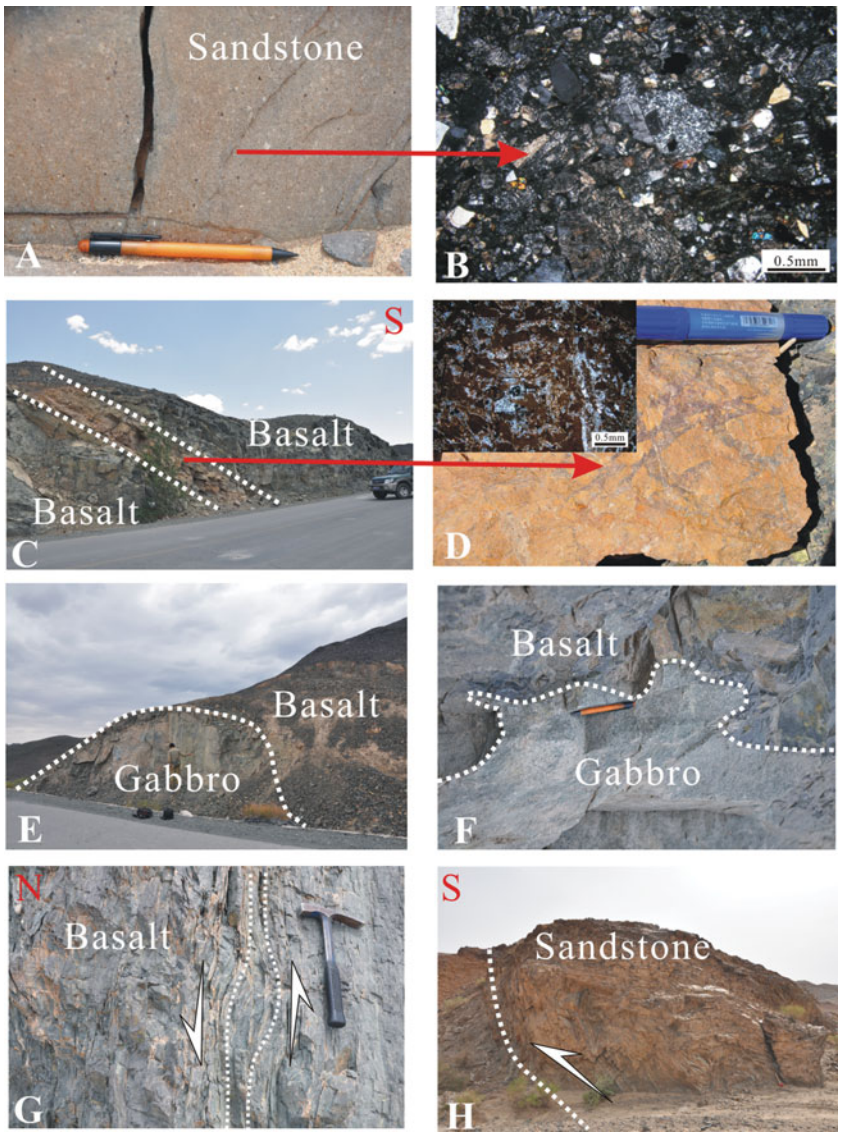

Figure 5. (Colour online) Photographs and microphotographs of typical sedimentary layers and structural features along the Liuyuan Volcanic Belt. (a) Pebbly sandstone on the south side of the Liuyuan Volcanic Belt. (b) Photomicrograph from (a); feldspar, quartz and volcanic clasts are included. (c) Sandstone and breccias between basalt layers, which was referred to as siliceous chert in Mao *et al.* (2012). (d) Surface of the sandstone and microphotographs from (c). (e) Intrusive relationship between gabbro and basalt in the southern part of the Liuyuan Volcanic Belt, also along cross-section A-A' (Fig. 4). (f) Intrusive relationship between gabbro and basalt in the northern part of the Liuyuan Volcanic Belt. (g) Basalt layers deformed by the strike-slip motion. (h) South-vergent fold-and-thrust fault deformation on the south side of the Liuyuan Volcanic Belt.

intruded into the basalts and sedimentary sequences (Fig. 3). A gabbro intrudes into the pillow lavas at Huitongshan Point (east of Gubaoquan), and the intrusive contact is clearly exposed. In the southern part of the Liuyuan cross-section, a fine-grained gabbro was intruded into pillow lavas. All of the volcanic rocks, as well as the sandstones beneath the volcanic rocks, have been unconformably overlain by the upper Permian – Lower Triassic reddish sandstones. Throughout the region, lamprophyre dykes have intruded parallel to the axial planes of folds; these dykes postdate all the metamorphic, sedimentary and intrusive rocks. Samples of these dykes have been collected from the southern side of the volcanic belt in order to constrain the timing of deformation.

3. Zircon U–Pb LA-ICP-MS geochronology

3.a. Analytical methods

Zircons were extracted using conventional separation techniques before hand-picking under a binocular microscope, mounting in epoxy resin and polishing to expose the zircon cores. The zircons were then imaged using cathodoluminescence (CL) and an electron microprobe to identify well-preserved and representative zircons for analysis. One or two analytical points on each zircon were used for trace-element analyses and U–Pb dating. Analyses of zircon trace-element compositions and some of the dating were performed by laser-ablation inductively coupled plasma mass spectrometer (LA-ICP-MS) at China University

https://doi.org/10.1017/S0016756815001077 Published online by Cambridge University Press

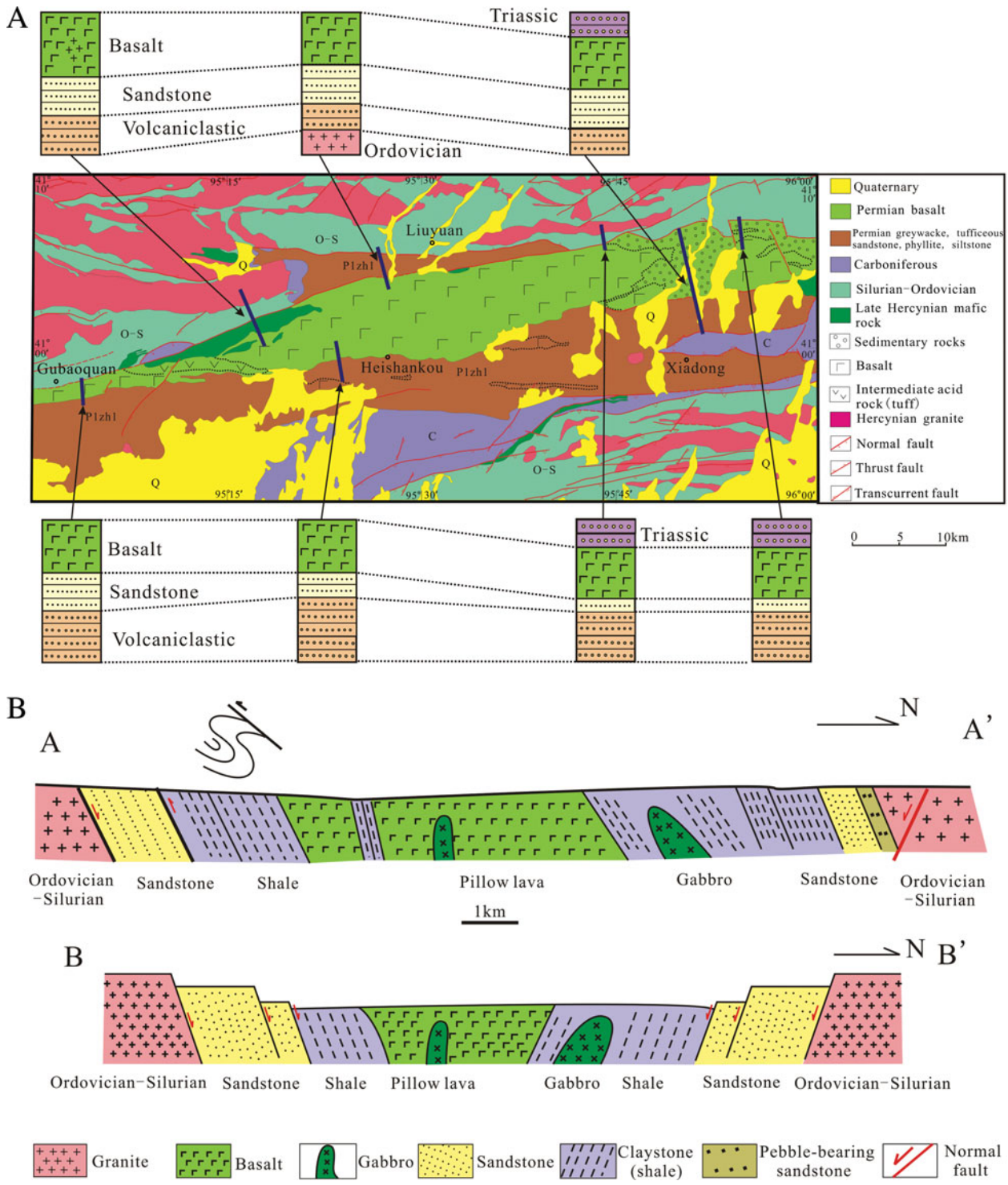

Figure 6. (Colour online) Sedimentary distributions and relationships between basalt and sandstone of the Liuyuan area. (a) Sedimentary profiles in different positions along the Liuyuan Volcanic Belt. (b) Summary cross-section of the present sedimentary rocks, basalt and gabbro (A–A') and potential Permian sedimentary section of the Liuyuan Volcanic Belt (B–B') (no scale). Q – Quaternary; P1zh – Early Permian Zheshi Formation; C – Carboniferous; O-S – Ordovician–Silurian.

of Geosciences, Wuhan, China using a *c.* 30 μm diameter spot size and the well-established laboratory procedures described by Liu *et al.* (2004). The rest of the dating was undertaken at the China University of Geosciences, Beijing, China. A 91500 zircon was used as an external standard during the age calculations and was measured every five or six analyses; in addition, the NIST SRM610 standard was analysed twice every 20 analyses of U, Th and Pb trace elements. U–Pb ages were calculated using ISOPLOT 3.23 (Ludwig, 2005).

3.b. Analytical results

A total of 22 samples of sandstone, gabbro, dacite, rhyolite and granite (Fig. 3) were collected to constrain the timing of eruption of the basalt,

https://doi.org/10.1017/S0016756815001077 Published online by Cambridge University Press

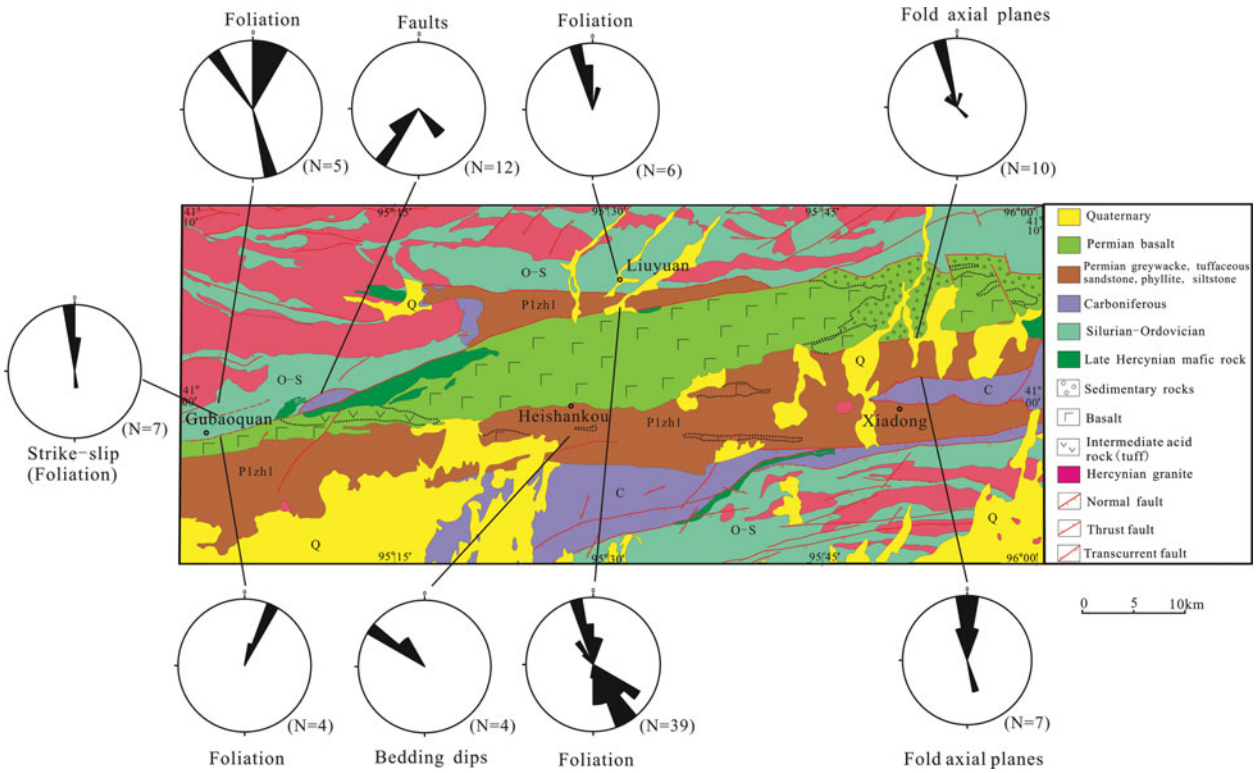

Figure 7. (Colour online) Structural features and kinematic directions on both the north and south sides of the Liuyuan Volcanic Belt. Inset equal: area lower hemisphere stereonets show fold, fault and foliations kinematics. As well as typical marked fold, fault and foliation, others are based on the bedding dips and foliations (parallel to sedimentary beds). Q – Quaternary; P1zh – Early Permian Zheshi Formation; C – Carboniferous; O-S – Ordovician–Silurian.

deposition of the sedimentary sequences, emplacement of the granites and deformation evidenced by syndeformational lamprophyre dykes. Data from individual samples are listed in Table 1, plotted in Figure 8 and online supplementary Figure S1 (available at http://journals.cambridge.org/geo) and are briefly described below. Data are listed in online supplementary Table S1 (available at http://journals.cambridge.org/geo).

3.b.1. *Detrital zircons*

Zircons from six sandstone samples were analysed, including one black sandstone sample (LY-25) from the top of the pillow lavas, two deformed sandstone samples (LY-76 and LY-56) on the south side of the Liuyuan Volcanic Belt and three deformed sandstone samples (LY-59, LY-89 and LY-92) on the north side.

Sample LY-25. A total of 24 spots were analysed from 24 zircon grains. The Th contents show a range of 88–651 ppm and U contents a range of 116–1489 ppm. The Th/U ratios are 0.12–1.50 (Table S1, available at http://journals.cambridge.org/geo). The analyses provide a wide range of ages over 641–231 Ma, among which five ages form the youngest group with a $^{206}Pb/^{238}U$ weighted mean age of 234 ± 10 Ma. Another two age clusters are 438 ± 19 Ma and 281 ± 11 Ma.

Sample LY-56. A total of 30 spots were analysed from 30 zircon grains. The Th contents show a range of 35–680 ppm and U contents a range of 85–1067 ppm. The Th/U ratios are 0.16–1.06 (Table S1, available at http://journals.cambridge.org/geo). The $^{206}Pb/^{238}U$ ages show a wide range over 1181–269 Ma. Eighteen spots define the youngest weighted mean $^{206}Pb/^{238}U$ age of 284 ± 7 Ma (MSWD = 6.9). Another group, including three analytical spots, yielded a weighted mean $^{206}Pb/^{238}U$ age of 429 ± 24 Ma.

Sample LY-76. A total of 120 spots were analysed from 120 zircon grains. The Th contents show a range of 27–2259 ppm and U contents a range of 118–3881 ppm. The Th/U ratios are 0.12–1.09 (Table S1, available at http://journals.cambridge.org/geo). The analyses can be clearly divided into two age groups, among which 37 form a coherent group with a concordia $^{206}Pb/^{238}U$ age of 285 ± 5 Ma (MSWD = 5.9). Another group, including 47 analytical spots, yielded a weighted mean $^{206}Pb/^{238}U$ age of 433 ± 7 Ma.

Sample LY-59. A total of 90 spots were analysed from 90 zircon grains. The Th contents show a wide range of 14–869 ppm and U contents a wide range of 26–1973 ppm. The Th/U ratios are 0.14–1.66 (Table S1, available at http://journals.cambridge.org/geo). The $^{206}Pb/^{238}U$ ages show a wide range over 2578–279 Ma. The data can mainly be divided into two age groups. One group with 24 spots yielded a weighted mean $^{206}Pb/^{238}U$ age of 293 ± 5 Ma (MSWD = 3.3). Another group with 48 analytical spots yielded a weighted mean $^{206}Pb/^{238}U$ age of 440 ± 6 Ma (MSWD = 4.1).

Sample LY-89. A total of 110 spots were analysed from 110 zircon grains. The Th contents show a range

https://doi.org/10.1017/S0016756815001077 Published online by Cambridge University Press

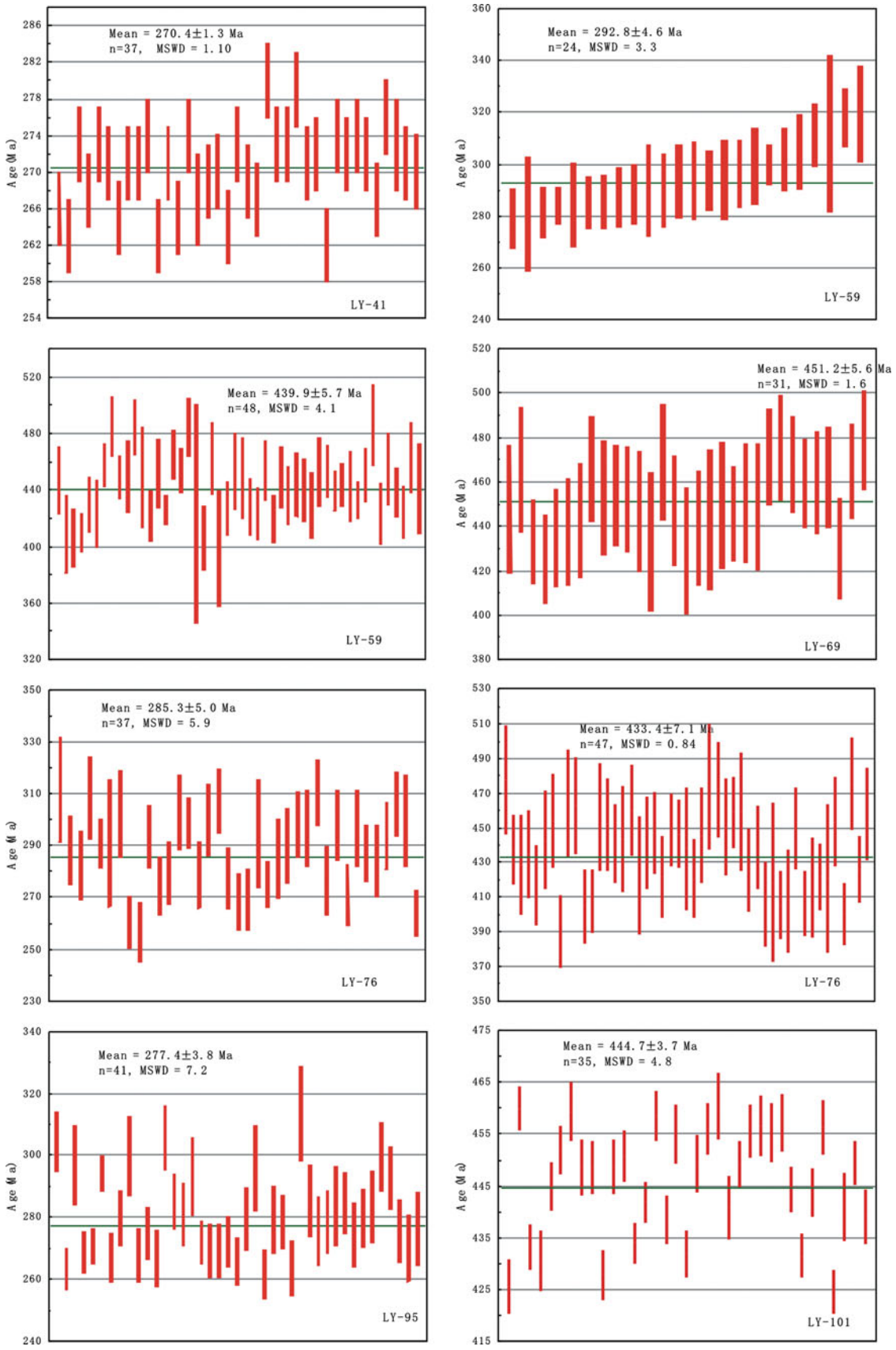

Figure 8. (Colour online) Part of zircon LA-ICP-MS age data plots and mean ages of $^{206}Pb/^{238}U$ for sedimentary rocks, volcanic rocks, gabbro and granite**.** Others are available in data repository.

https://doi.org/10.1017/S0016756815001077 Published online by Cambridge University Press

Table 1 Sampled sites, petrologic descriptions and zircon age data in Liuyuan area

Sampled number	Latitude and longitude	Petrologic descriptions	Positions in the field	$^{206}Pb/^{238}U$ mean age (Ma)
LY-20	41° 01′ 17″ N, 95° 28′ 12″ E	Volcanic clastics (top of the pillow lava)	S. Liuyuan	268 ± 9 Ma, 429 ± 17 Ma
LY-22	41° 01′ 32″ N, 95° 28′ 13″ E	gabbro	S. Liuyuan	404 ± 14 Ma
LY-25	41° 01′ 39″ N, 95° 28′ 12″ E	Black sandstone (top of pillow lava)	S Liuyuan	234 ± 10 Ma, 281 ± 11 Ma, 438 ± 19 Ma
LY-41	41° 03′ 46″ N, 95° 28′ 20″ E	Gabbro	S Liuyuan	270 ± 1 Ma
LY-45	41° 01′ 17″ N, 95° 09′ 00″ E	Mylonite	N Huitongshan	926 ± 15 Ma
LY-56	40° 57′ 56″ N, 95° 09′ 58″ E	Sandstone	S Huitongshan	284 ± 7 Ma, 429 ± 24 Ma
LY-59	41° 04′ 55″ N, 95° 27′ 21″ E	Sandstone	N Liuyuan	293 ± 5 Ma, 440 ± 6 Ma
LY-65	41° 05′ 42″ N, 95° 26′ 45″ E	Mylonitized diorite	N Liuyuan	466 ± 7 Ma
LY-69	40° 59′ 43″ N, 95° 08′ 54″ E	Granite	Huitongshan	451 ± 6 Ma
LY-74	40° 58′ 56″ N, 95° 07′ 19″ E	O-S schist	Huitongshan	457 ± 33 Ma
LY-75	40° 58′ 55″ N, 95° 07′ 20″ E	Granitic lens	Huitongshan	895 ± 15 Ma
LY-76	41° 01′ 33″ N, 95° 41′ 53″ E	Sandstone	Xiadong	285 ± 5 Ma, 433 ± 7 Ma
LY-77	41° 01′ 35″ N, 95° 41′ 53″ E	Lam (dyke)	Xiadong	227 ± 7 Ma
LY-81	41° 05′ 46″ N, 95° 43′ 02″ E	Siliceous rock	Xiadong	272 ± 34 Ma (not good)
LY-88	41° 06′ 21″ N, 95° 56′ 48″ E	Dacite	Xiadong	280 ± 4 Ma, 424 ± 19 Ma
LY-89	41° 06′ 21″ N, 95° 56′ 48″ E	Dacite	Xiadong	279 ± 3 Ma, 438 ± 10 Ma
LY-92	41° 07′ 07″ N, 95° 50′ 05″ E	Sandstone on the O-S schist (boundary)	West of Xiadong	285 ± 5 Ma, 442 ± 5 Ma
LY-94	41° 06′ 52″ N, 95° 48′ 16″ E	Granite (intruded by diabase dykes)	West of Xiadong	422 ± 5 Ma
LY-95	41° 05′ 54″ N, 95° 48′ 19″ E	Rhyolite	West of Xiadong	277 ± 4 Ma
LY-101	41° 04′ 24″ N, 95° 16′ 15″ E	Granite (intruded by diabase dykes)	Huitongshan	445 ± 4 Ma
LY-108	41° 00′ 32″ N, 95° 14′ 38″ E	Fine-grain gabbro	Huitongshan	280 ± 6 Ma
LY-122	41° 04′ 08″ N, 95° 29′ 13″ E	Gabbro	S Liuyuan	277 ± 3 Ma

of 65–2185 ppm and U contents a range of 169–4049 ppm. The Th/U ratios are 0.07–1.35 (Table S1, available at http://journals.cambridge.org/geo). Excluding 22 spots, the remaining 88 can be divided into two age groups: one with 57 spots yielded a weighted mean $^{206}Pb/^{238}U$ age of 279 ± 3 Ma (MSWD = 3.3); and another with 31 analytical spots yielded a weighted mean $^{206}Pb/^{238}U$ age of 438 ± 10 Ma (MSWD = 5.3).

Sample LY-92. A total of 110 spots were analysed from 110 zircon grains. The Th contents show a wide range of 20–9525 ppm and U contents a wide range of 66–6307 ppm. The Th/U ratios are 0.07–2.45 (Table S1, available at http://journals.cambridge.org/geo). The analyses can also be divided into two age groups: one with 29 spots yielded a weighted mean $^{206}Pb/^{238}U$ age of 285 ± 5 Ma (MSWD = 4.4) and another with 62 spots yielded a weighted mean $^{206}Pb/^{238}U$ age of 442 ± 5 Ma.

In summary, the data described above indicate that: (1) there are two clusters of detrital zircon ages on the northern side of the Liuyuan Volcanic Belt (293–279 and 442–438 Ma), and two clusters on the southern side (285–284 and 429–417 Ma); and (2) the sandstone at the top of the pillow lavas was deposited after 234 ± 10 Ma.

3.b.2. *Volcanic rocks*

Zircons from four volcanic samples were analysed, including one volcanic conglomerate sample (LY-20) from the top of the pillow lavas in south Liuyuan, two dacite samples (LY-88 and LY-81) from the east of Liuyuan Town (Xiadong valley) and one rhyolite sample (LY-95) from the east of Liuyuan Town (west of Xiadong valley).

Sample LY-20. A total of 17 spots were analysed from 17 zircon grains. The Th contents show a wide range of 41–3410 ppm and U contents a wide range of 104–6263 ppm. The Th/U ratios are 0.26–1.20 (Table S1, available at http://journals.cambridge.org/geo). The $^{206}Pb/^{238}U$ ages show a range of 1407–119 Ma. Four spots yielded a weighted mean $^{206}Pb/^{238}U$ age of 268 ± 9 Ma (MSWD = 0.62), and another four spots yielded a weighted mean $^{206}Pb/^{238}U$ age of 429 ± 17 Ma (MSWD = 0.69).

Sample LY-88. A total of 39 spots were analysed from 39 zircon grains. The Th contents show a wide range of 32–7244 ppm and U contents a wide range of 82–14452 ppm. The Th/U ratios are 0.17–1.11. The $^{206}Pb/^{238}U$ ages show a range of 440–218 Ma. Excluding 10 analyses, 29 spots yielded a weighted mean $^{206}Pb/^{238}U$ age of 280 ± 4 Ma (MSWD = 2.2). Five of the other 10 analyses yielded a weighted mean $^{206}Pb/^{238}U$ age of 424 ± 19 Ma (MSWD = 0.27). The other five analyses yielded a mix of ages over the range 400–300 Ma.

Sample LY-81. The zircons in this siliceous rock are too small to analyse with any precision. We attempted to analyse eight spots, and their Th contents showed a wide range of 144–5529 ppm and the U contents a wide range of 197–5090 ppm. The Th/U ratios are 0.18–1.75. The $^{206}Pb/^{238}U$ ages showed a wide range of 913–215 Ma.

Sample LY-95. A total of 44 spots were analysed from 44 zircon grains. The Th contents show a range of 29–3433 ppm and U contents a range of 79–1935 ppm.

https://doi.org/10.1017/S0016756815001077 Published online by Cambridge University Press

The Th/U ratios are 0.36–1.77. Excluding 3 spots, the remaining 41 spots yielded a weighted mean $^{206}Pb/^{238}U$ age of 277 ± 4 Ma (MSWD = 7.2).

In summary, the data described above indicate that the volcanic rocks formed at *c.* 280–270 Ma.

3.b.3. *Gabbros*

The zircons from four gabbro samples were analysed, including three gabbro samples (LY-22, LY-41 and LY-122) from south of Liuyuan Town and one gabbro sample (LY-108) from Huitongshan (east of Gubaoquan), west of Liuyuan Town.

Sample LY-22. A total of 11 spots were analysed from 11 zircon grains. The Th contents show a range of 45–651 ppm and U contents a range of 107–1298 ppm. The Th/U ratios are 0.19–0.68 (Table S1, available at http://journals.cambridge.org/geo). Excluding 1 core age of 1844 ± 21 Ma, the remaining 8 spots yielded a weighted mean $^{206}Pb/^{238}U$ age of 404 ± 14 Ma (MSWD = 0.76).

Sample LY-41. A total of 37 spots were analysed from 37 zircon grains. The Th contents show a range of 125–3036 ppm and U contents a range of 187–1902 ppm. The Th/U ratios are 0.60–1.74 (Table S1, available at http://journals.cambridge.org/geo). The 37 spots yielded a weighted mean $^{206}Pb/^{238}U$ age of 270 ± 1 Ma (MSWD = 1.1).

Sample LY-108. A total of 30 spots were analysed from 30 zircon grains. The Th contents show a range of 14–719 ppm and U contents a range of 24–602 ppm. The Th/U ratios are 0.45–1.19 (Table S1, available at http://journals.cambridge.org/geo). Excluding 10 mixed or discordant ages, the remaining 20 spots yielded a weighted mean $^{206}Pb/^{238}U$ age of 280 ± 6 Ma (MSWD = 0.34).

Sample LY-122. A total of 35 spots were analysed from 35 zircon grains. The Th contents show a range of 14–6141 ppm and U contents a range of 27–1937 ppm. The Th/U ratios are 0.46–3.17 (Table S1, available at http://journals.cambridge.org/geo). Thirty-three spots yielded a weighted mean $^{206}Pb/^{238}U$ age of 277 ± 3 Ma (MSWD = 2.1).

In summary, the data described above indicate that the gabbro formed at *c.* 280–270 Ma.

3.b.4. *Granitic plutons and schists*

The zircons from three granitic rocks and three schist samples were analysed, including mylonite (LY-45) and mylonitized diorite (LY-65) from north of Liuyuan Town, granites (LY-69 and LY-101) and Ordovician–Silurian schist (LY-74) from Huitongshan (east of Gubaoquan) and granite (LY-94) from west of Xiadong valley.

Sample LY-45. A total of 28 spots were analysed from 28 zircon grains. The Th contents show a range of 63–1457 ppm and U contents a range of 298–1620 ppm. The Th/U ratios are 0.11–1.03 (Table S1, available at http://journals.cambridge.org/geo). Excluding two old ages from zircon cores, the remaining 26 spots yielded a weighted mean $^{206}Pb/^{238}U$ age of 926 ± 15 Ma (MSWD = 0.75).

Sample LY-65. A total of 68 spots were analysed from 68 zircon grains. The Th contents show a range of 77–977 ppm and U contents a range of 159–1257 ppm. The Th/U ratios are 0.39–1.32 (Table S1, available at http://journals.cambridge.org/geo). Excluding 13 old zircon core ages, mixed ages or discordant ages, the remaining 55 spots yielded a weighted mean $^{206}Pb/^{238}U$ age of 466 ± 7 Ma (MSWD = 2.6).

Sample LY-69. A total of 35 spots were analysed from 35 zircon grains. The Th contents show a range of 242–1553 ppm and U contents a range of 380–6873 ppm. The Th/U ratios are 0.18–1.18 (Table S1, available at http://journals.cambridge.org/geo). Excluding three slightly older or younger ages, the remaining 31 spots yielded a weighted mean $^{206}Pb/^{238}U$ age of 451 ± 6 Ma (MSWD = 1.6).

Sample LY-74. A total of 25 spots were analysed from 25 zircon grains. The Th contents show a range of 1–885 ppm and U contents a range of 46–3154 ppm. The Th/U ratios are 0.001–0.61 (Table S1, available at http://journals.cambridge.org/geo). The $^{206}Pb/^{238}U$ ages show a range of 1459–392 Ma. Five spots yielded a weighted mean $^{206}Pb/^{238}U$ age of 457 ± 33 Ma (MSWD = 4.9). The other spot analyses represent old cores or mixed ages.

Sample LY-94. A total of 29 spots were analysed from 29 zircon grains. The Th contents show a range of 107–493 ppm and U contents a range of 294–3106 ppm. The Th/U ratios are 0.08–1.25 (Table S1, available at http://journals.cambridge.org/geo). Excluding two younger ages and two older ages, 25 spots yielded a weighted mean $^{206}Pb/^{238}U$ age of 422 ± 5 Ma (MSWD = 1.6).

Sample LY-101. A total of 35 spots were analysed from 35 zircon grains. The Th contents show a range of 293–1844 ppm and U contents a range of 712–3047 ppm. The Th/U ratios are 0.34–0.67 (Table S1, available at http://journals.cambridge.org/geo). The 35 spots yielded a weighted mean $^{206}Pb/^{238}U$ age of 445 ± 4 Ma (MSWD = 4.8).

In summary, the granite from Huitongshan yielded an age of 451 ± 6 Ma and was intruded by mafic dykes. The mylonites and mylonitized diorites yielded ages of 926 ± 15 and 466 ± 7 Ma, respectively. The Ordovician–Silurian schist from Huitongshan yielded an age of 457 ± 33 Ma.

3.b.5. *Granitic and lamprophyre dykes: zircon LA-ICP-MS geochronology*

The zircons from two dykes were analysed, including a granitic dyke (LY-75) from Huitongshan and a lamprophyre dyke (LY-77) from Xiadong.

Sample LY-75. A total of 30 spots were analysed from 30 zircon grains. Excluding two discordant ages, the 28 spots yielded a weighted mean $^{206}Pb/^{238}U$ age of 895 ± 15 Ma (MSWD = 0.81).

https://doi.org/10.1017/S0016756815001077 Published online by Cambridge University Press

Sample LY-77. A total of 32 spots were analysed from 32 zircon grains. The Th contents show a range of 131–3383 ppm and U contents a range of 55–5105 ppm. The Th/U ratios are 0.33–3.69 (Table S1, available at http://journals.cambridge.org/geo). Twelve spots yielded a weighted mean $^{206}Pb/^{238}U$ age of 227 ± 7 Ma (MSWD = 5.8). The other ages included the oldest zircon core age of 1701 ± 174 Ma and various mixed ages.

3.c. Interpretation of the zircon U–Pb age data

Previous works have reported ages for some of the gabbros in the Liuyuan area and adjacent regions (e.g. 281 Ma, Ao *et al.* 2010), as well ages for granitic plutons (e.g. 275 Ma, Qin *et al.* 2011). These data are derived from different areas, and were not presented in the context of a clear time sequence. For our study, we focused on the various lithologies in the Liuyuan area and examined the granites and schists, the overlying sandstones, claystones, volcaniclastics, gabbros, dacites, rhyolitic tuffs and also the reddish-coloured sandstones that lie on top of all the other sequences (Table 1; Fig. 9).

The surrounding areas of granite and schist on both sides of the Liuyuan Volcanic Belt yield ages older than the basaltic pillow lava and associated volcanic rocks. They therefore represent former island-arc rocks rather than the subduction zone materials that might have formed in association with the closure of the Palaeo-Asian Ocean during Ordovician–Silurian time; our data do not indicate that they represent an ophiolite complex of Permian age. The granitic rocks to the north of the Liuyuan Volcanic Belt have ages of 466–422 Ma, and all of them have undergone thermal metamorphism. The basement of the region, represented by granitic lenses and mylonites, yielded ages of 926 and 895–860 Ma, respectively, and these ages are consistent with existing age data for the Dunhuang-Alxa crystalline basement (e.g. Geng & Zhou, 2011).

Identical or similar age clusters of the detrital zircons exist on both the southern and northern sides of the Liuyuan Volcanic Belt, but the ages within the 290–285 Ma clusters young from north to south (Fig. 3). There are two clusters of detrital zircon ages on the north side (293–285 and 440–450 Ma) and two on the south side (290–280 and 440–430 Ma). On the northern side of the zone, the younger age cluster is somewhat earlier than on the southern side by *c.* 1–2 Ma. The eruptions of tuff and volcaniclastic material pre-dated the gabbros, dacites and rhyolites by *c.* 2–10 Ma. The mafic intrusive activity took place at the same time as the acid magmatic eruptions of dacite and rhyolite, and is later than the volcaniclastics.

Our detrital zircon age data show that the sandstones close to the basalt formed later than those further away that carry younger zircon ages. An example is sample LY-92 which has a cluster of zircon ages at *c.* 286 Ma ($^{206}Pb/^{238}U$ mean ages), with a youngest age of 279 Ma that is close to, but slightly younger than, the age of the basalt. The deposition of the tuffs in the Liuyuan Volcanic Belt took place during 290–280 Ma, from the margin to the centre of the sedimentary depression.

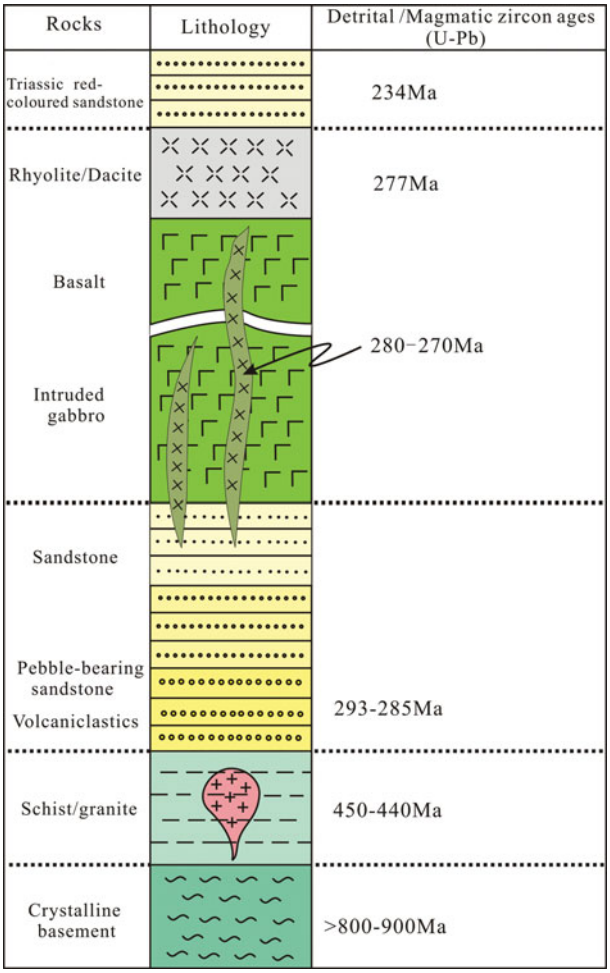

Figure 9. (Colour online) Summary sedimentary profiles and relationships between basalt and gabbro. Age data are from this study.

The ages of zircons in the gabbros are younger than the ages of detrital zircon from the sandstones, but they are similar to the ages of zircons from the rhyolites and dacites. They mainly range over 280–277 Ma, but the youngest gabbro that cuts all the pillow lavas has an age of 272 Ma. Some of the gabbros are therefore somewhat younger than the dacites (277 Ma) and rhyolites (277 Ma).

Continuous sedimentation on top of the pillow lava basalts was taking place at *c.* 234 Ma, corresponding to the regional depression in Tianshan and other areas in the northern margin of Chinese continent. After this period of subsidence, intracontinental deformation occurred. The lamprophyre dykes yielded ages of 230–227 Ma, and are therefore contemporaneous or slightly younger than the intracontinental deformation. These dykes were emplaced parallel to the axial planes of folds, which constrains the time of formation of the east–west-trending folds and thrust deformation in the region.

https://doi.org/10.1017/S0016756815001077 Published online by Cambridge University Press

4. Discussion

4.a. Lack of evidence for oceanic sedimentation and ophiolite complex

Mao *et al.* (2012), Xiao *et al.* (2009, 2010) and Xiao, Sun & Santosh (2015) proposed that the Liuyuan Volcanic Belt represents an ophiolite complex based on the following observations: chert layers within the pillow lava basaltic series; numerous thrust faults; a thrust relationship between the gabbros and the pillow lavas; Permian island-arc magmatic systems on both the northern and southern sides of the Liuyuan Volcanic Belt; and the presence of so-called MORB basalt. However, our detailed field investigations do not support these inferences. The siliceous cherts and gabbros derived from oceanic lithosphere are conspicuously absent. Also, the thrust system related to the ophiolite complex is not found. We address these aspects in more detail below.

Firstly, there is no evidence of an oceanic environment in the Liuyuan Volcanic Belt: there are no oceanic sediments and no marine fossils. The pillow lavas occurring in this area could just as well have formed under fresh water (Yamagishi, 1985; Kawachi & Pingle, 1988). The sediments on both sides of the volcanic belt are comparable, and the nature of the sandstones and claystones from the margins to the centre of the rift clearly show that the Liuyuan region was not an ocean or an oceanic ridge. There are no limestones or dolomitic rocks, and the muddy carbonates are consistent with a lacustrine environment. The rock that Mao *et al.* (2012, fig. 4a, e) described as chert is in fact sandstone and pebbly sandstone.

Secondly, there is no thrust relationship between the gabbroic intrusions and the pillow lavas (e.g. Kennish & Lutz, 1998; Shaker Ardakani *et al.* 2009), and the ophiolitic features reported by Mao *et al.* (2012) are absent in our area. Our detailed cross-sections drawn from field data show a lack of thrusting. What had previously been described as a thrust fault is actually a gravity collapse feature (Mao *et al.* 2012, fig. 4a).

Thirdly, the granites and schists (that have island-arc characteristics) on both sides of the pillow-lava basalts are Ordovician–Silurian in age (450–440 Ma) as shown by our age data, far older than the 290–280 Ma Liuyuan pillow lavas, and it is clear from field relationships that the pillow lavas overlie the older Ordovician–Silurian granites and schists. There is therefore no evidence that the formation of the Liuyuan pillow-lava basalts was related to an island arc (not even a Permian island arc) or a subduction zone, and it is possible that there was never an oceanic realm within which the Liuyuan lavas were erupted.

Finally, we note that the Ar–Ar and Rb–Sr data of Mao *et al.* (2012), which gave ages of *c.* 230–220 Ma for the granites and schists, are cooling ages. In contrast, our zircon U–Pb ages of 450–440 Ma for these rocks represent an island arc that formed at 450–440 Ma and not 230–220 Ma. So far, granites with ages of 230–220 Ma have not been found in the Liuyuan Volcanic Belt and adjacent regions either in our study or in previous work.

We therefore conclude that there is no evidence for an ophiolite complex or an island arc that is related to the Permian Liuyuan pillow lavas. The Ordovician and Silurian granites and schists were formed in relation to earlier episodes of active tectonics along a continental margin that involved the microcontinental Dunhuang-Alxa Block. The northern and southern sides of the Liuyuan pillow-lava belt, composed of older granites and schists, were certainly connected to each other, but the region started to rift in the Permian. A lake was created in which the various sediments described above were deposited and where the pillow lavas erupted. The volcanic belt includes not only pillow-lava basalt, but dacites and rhyolites.

Previous studies have described the pillow lavas as MORB types (Xiao *et al.* 2010; Mao *et al.* 2012), and it seems clear that the basalts and related gabbros have trace-element and isotopic Nd and Sr compositions that are close to those of MORB (Zhao *et al.* 2004, 2006; Jiang *et al.* 2007; Mao *et al.* 2012). In fact, there are two end-members of OIB and MORB, with MORB being the main end-member (Liu, Zhao & Guo, 2006; Zhao *et al.* 2006; Pan, Guo & Zhao, 2008; Zhang *et al.* 2011, 2012). However, these basalts lie between basalt and trachybasalt on SiO_2–K_2O plots (Jiang *et al.* 2007). Notably, in addition to the basalt there are felsic rocks (including tuffs and dacite), suggesting that the rift volcanic rocks constitute a bimodal volcanic series. The magma would have formed from depleted mantle, perhaps asthenospheric mantle (Jiang *et al.* 2007), but the rocks would not have formed at an oceanic ridge or in association with a subduction-related fore-arc or back-arc (such as the SSZ, as was proposed by Mao *et al.* 2012).

4.b. Tectonic setting and evolution

The results presented in our study from Liuyuan and nearby areas can be used to reconstruct the following tectonic history (Figs 10, 11). (1) The presence of a 900 Ma Dunhuang-Alxa crystalline basement indicates that the basement of the Liuyuan rift system was an old active continental margin. (2) The 450–440 Ma granites and schists on the northern and southern sides of the Liuyuan Volcanic Belt formed the continental margin when the Liuyuan Volcanic Belt was formed, and they represent an earlier island arc. (3) The rapid sedimentation on both sides of the Liuyuan Belt, and the sequences of coarse- to fine-grained sediment, are consistent with the opening of a rift with sedimentation from both sides. (4) Eventually, deeper-water claystones and pillow-lava basalts formed in the rift zone. (5) At a late stage, dacites and rhyolites formed (Fig. 10); at the same time (or slightly later) the fine- and coarse-grained gabbros and olivine gabbros were intruded into the sandstones and pillow-lava basalts (older than 280 Ma). (6) From 280 until 234 Ma there is no record of any sedimentation

https://doi.org/10.1017/S0016756815001077 Published online by Cambridge University Press

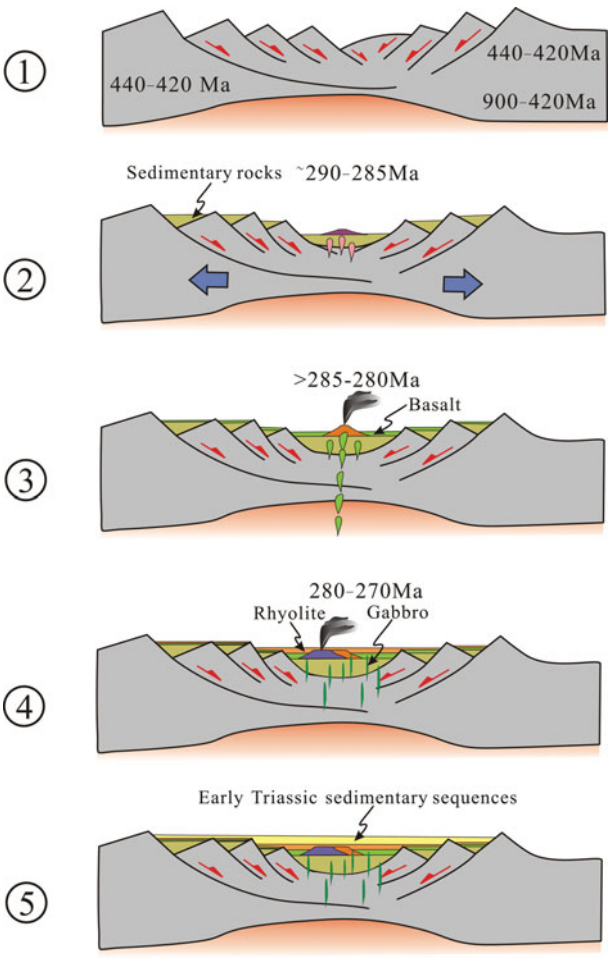

Figure 10. (Colour online) Tectonic evolution from *c.* 440 Ma to the Mesozoic Era. Cross-sections showing the formation and evolution of the rift system in the Liuyuan area. Magmatic upwelling resulted in basaltic and other volcanic eruptions, and the formation of a rift sedimentary environment.

in the Liuyuan rift but, regionally, strike-slip movements and the extrusion of Tianshan Block took place during 270–245 Ma (Wang *et al.* 2005; Wang, Li & Sun, 2008; Wang, Sun & Li, 2010) and the tectonic framework changed during *c.* 245–230 Ma when the CAOB was extruded eastwards and the Palaeo-Tethys intracontinental deformation occurred (Fig. 11b). (7) Subsequently, the Early Triassic reddish-coloured sediments (younger than 234 Ma) were deposited disconformably over the above-mentioned sedimentary and metamorphic rocks. Later at 230–227 Ma, strike-slip motions and north–south-compression together resulted in transpression throughout the region (Fig. 11b). After rifting and post-rift sedimentation and volcanism, north- and south-verging folds and some thrust faults formed, significantly modifying the regional tectonic framework. Meanwhile, lamprophyre dykes intruded at 230–227 Ma, parallel to the axial planes of folds, and the age of these dykes constrains the age of the earlier deformation. Strike-slip motions continued during this time, including those on the Xingxingxia ductile sinistral strike-slip fault and the Altyn Tagh sinistral strike-slip fault (Wang *et al.* 2005; Wang, Sun & Li, 2010). At the same time, regional contraction combined with sinistral strike-slip motion produced folds that verge north and south, as well as thrust faulting. None of the adjacent regions display the same pattern of deformation, and the tectonic activity in the Liuyuan Volcanic Belt is unrelated to the Triassic closure of the Palaeo-Asian Ocean (Mao *et al.* 2012), but can be more logically explained by intracontinental deformation in response to a far-field north–south contraction (Wang *et al.* 2005; Wang, Sun & Li, 2010). Moreover, in Tianshan and adjacent regions, there is no north–south compression with only strike-slip movements at this time interval.

In terms of the broader tectonic setting and dynamics, the 450–440 Ma granites and schists might be related to the closing of an Ordovician–Silurian ocean. Subsequent to this event, there is no evidence for sedimentation and deformation in this region that could be related to the lost tectonic boundary of the closing oceanic realm related either to the Qilianshan region or the central Tianshan Orogenic Belt. Deformation in the Tianshan Orogenic Belt ended at 280 Ma, and prior to this there were WSW–ENE-trending sinistral strike-slip motions during 300–290 Ma together with north–south-compression in the central Tianshan region (Laurent-Charvet *et al.* 2002; Yang *et al.* 2007; Wang, Li & Sun, 2008; Wang, Sun & Li, 2010; Han *et al.* 2011). At the same time, the large-scale Tarim basalt province formed at 290–275 Ma (Zhang *et al.* 2013, 2014; Tian *et al.* 2014; Xu *et al.* 2014; Yang *et al.* 2015), followed by several granitic intrusions either coevally or later than these basaltic eruptions over the whole of Tianshan, Beishan and other regions (e.g. Han *et al.* 2011). The Tarim volcanic eruptions have been linked to a mantle plume (Zhou *et al.* 2004; Zhang *et al.* 2013, 2014). In the Liuyuan area and more widely in the CAOB and connected areas, several distinct tectonic domains can therefore be recognized prior to 300 Ma and post 230 Ma. During the period 300–230 Ma, the broad region was possibly an assemblage of continents within which the Liuyuan rift system formed.

With respect to the sedimentary environment of the Liuyuan rift, the nature of the sediments and the detrital zircon ages clearly show that this is a rift system with the sediments deposited in lacustrine (rather than marine) environment. Furthermore, we have shown that the rift was located on a continental margin, and that the rifting was accompanied by basaltic and eventually dacite and rhyolite eruptions, representing a bimodal suite that is consistent with rift magmatism. The Santanghu volcanic eruptions (NW of the Liuyuan area) (Han *et al.* 1998; Zhao *et al.* 2006) could be connected in time and space to the same delamination that may have occurred after the formation of the Tianshan–Beishan Orogen. However, the eruption of the Tarim basalts, and some other basalts along the earlier continental margin, cannot be correlated to lithospheric delamination.

As we exclude the ophiolite complex hypothesis in this study, we need to reconsider the magmatic sources for these volcanic eruptions such as lithosphere, mantle plume or subduction-related. The

https://doi.org/10.1017/S0016756815001077 Published online by Cambridge University Press

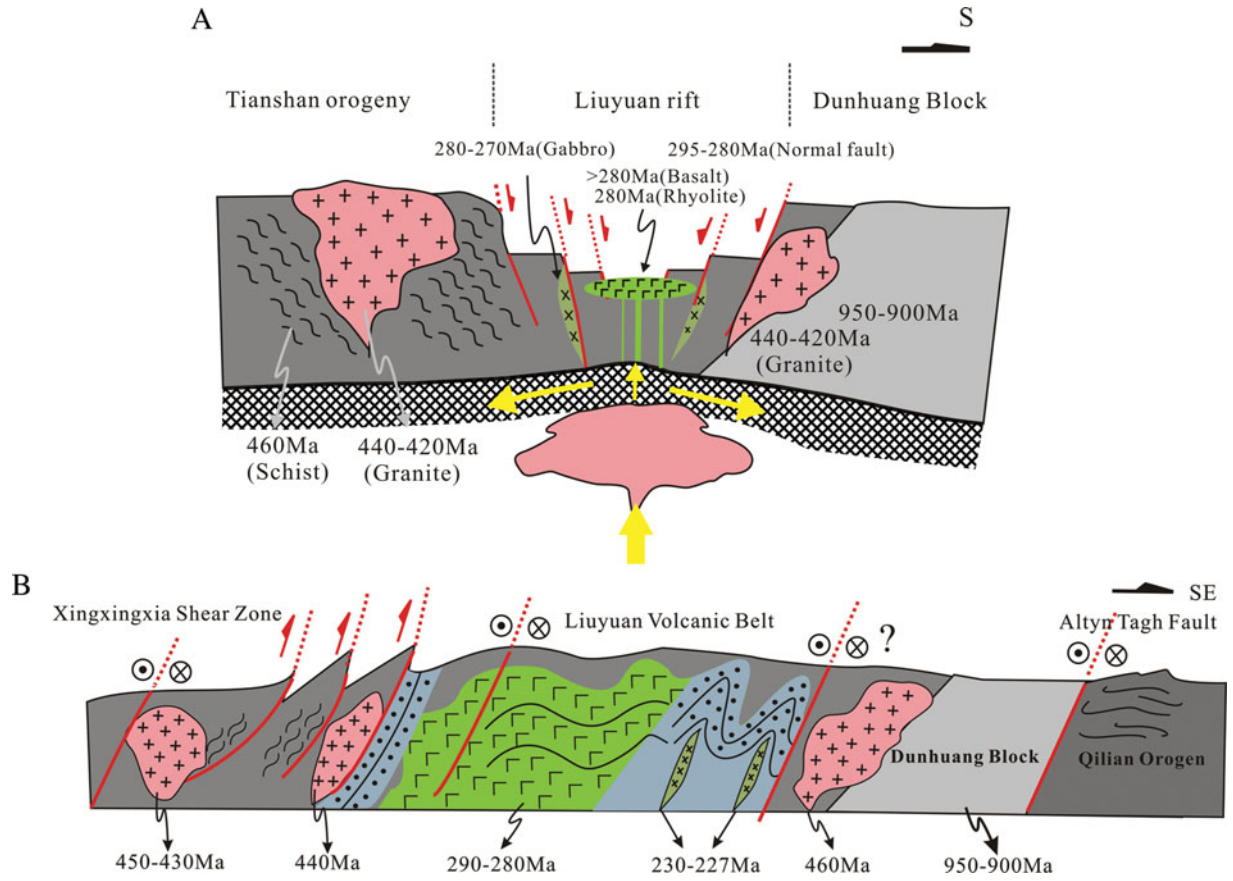

Figure 11. (Colour online) Tectonic background of the Liuyuan rift formation and deformation. (a) Summary cross-section of structural relationships and sedimentary sequences during the rift formation, as well as the tectonic background. (b) South-verging fold-and-thrust deformation during 230–227 Ma. Lamprophyre dykes were intruded along the axial planes of the folds. Age data are from this study.

magmatic sources usually considered for volcanic eruptions in rift-depressions are: (1) interaction of the crust and mantle accompanied by delamination during orogenesis (Han *et al.* 1998; Jiang *et al.* 2006, 2007); or (2) upwelling of the lithospheric mantle resulting in crust–mantle interactions, the formation of rifts and magma sourced from asthenosphere.

4.c. Regional temporal and spatial distribution of Permian volcanic eruptions

Volcanic eruptions took place in the Tarim Block and along its northern margin, as well as within the Tianshan–Beishan – Inner Mongolia orogenic belts at around the same time during Permian time (Han *et al.* 1998; Qin *et al.* 2011; J. B. Zhu, unpub. Ph.D. thesis, Chinese Academy of Geological Sciences, Beijing, 2015). Geochemical data indicate that those volcanic rocks are OIB and not MORB. However, a volcanic belt formed along the northern margins of the Tarim, Dunhuang-Alxa and North China Craton continental blocks (Fig. 12), with similar rift sedimentary environments in each case. Permian post-orogenic OIB-type intraplate basalts also occur in the southern Kyrgyz Tienshan (Simonov *et al.* 2015). Their continental intraplate origin has been well established.

Regionally, from the northern margin of the Tarim Block to the northern flanks of the Dunhuang and Alxa blocks and the northern North China Craton, the volcanic eruptions tend to be older (290–280 Ma) in the west and younger (285–270 Ma) (J. B. Zhu, unpub. Ph.D. thesis, Chinese Academy of Geological Sciences, Beijing, 2015) in the east, and sometimes as young as 260 Ma (Fig. 12a). The eruptions ranged from felsic to intermediate to mafic in composition in zones that were wider in the west and narrower in the east, and extending in the east to the northern margin of the China continent. These volcanic belts became active after the formation of the Tianshan – Inner Mongolia Orogenic Belt and after the amalgamation of the CAOB. The volcanic belts occupy a typical tectonic position with continental blocks to the south and orogenic belts to the north. Some of the volcanic eruptions were on old crystalline basement, but others occur within the orogenic belt. Reactivation and re-opening or local extension in the region could have produced the linear features that characterize these types of volcanic eruptions. Therefore, these volcanic belts cannot be interpreted in terms of orogenic processes or lithospheric delamination, or through a mantle plume model. Instead, they seem to represent a local extension that occurred during the process of the assembly of continental blocks. The convergence of several continents or blocks took place in the central Asia continent at the same time as the formation of Pangea (*c.* 320–250 Ma), and palaeomagnetic pole positions clearly show that numerous continental blocks collided with the Siberian continent during Palaeozoic time (Cocks *et al.* 2007; Wang *et al.* 2015).

https://doi.org/10.1017/S0016756815001077 Published online by Cambridge University Press

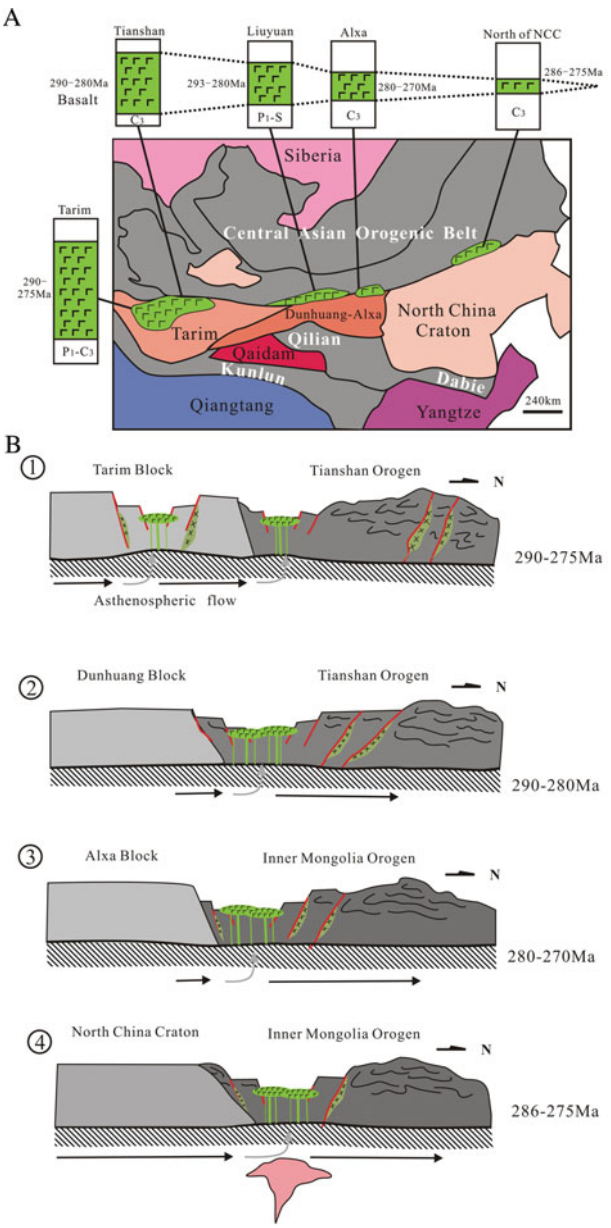

Figure 12. (Colour online) Regional characteristics and distribution of the 290–270 Ma volcanic zones. (a) 290–270 Ma volcanic rocks distributed along the northern margin of the China continent, including Tarim (290–275 Ma), Tianshan (290–280 Ma), Liuyuan (293–280 Ma), Alxa (280–270 Ma) and the North China Craton (286–275 Ma). Age data are from Zhang *et al.* (2013), J. B. Zhu (unpub. Ph.D. thesis, Chinese Academy of Geological Sciences, Beijing, 2015) and this study. (b) Cross-sections showing the volcanic eruptions and their tectonic background: 1, volcanic eruptions formed in the Tarim and Tianshan orogenic belts; 2, volcanic eruptions occurred between the Dunhuang Block and Tianshan Orogenic Belt; 3, volcanic eruptions occurred between the Alxa Block and the Inner Mongolia Orogenic Belt; and 4, volcanic eruptions formed between the North China Craton and Inner Mongolia Orogenic Belt.

During the same time interval, volcanic belts and large igneous provinces formed in the broader region, either in association with subduction at continental margins or as a result of local extension along the margin or within the interiors of the continental blocks (Fig. 12b). The overall regional tectonic stress regime was one of contraction, but locally there was extension and the eruption of volcanics with OIB composition. The sedimentary environment in these areas of local extension was that of a rift depression, and not that of a foreland or orogen. At the same time, asthenospheric flow occurred during this process and resulted in the interaction of the crust and mantle. In terms of the overall tectonics the continental margins and interiors, as well as previous island arcs or orogenic belts, were reactivated or reworked during the period of volcanic eruptions and rifting. We therefore envisage intracontinental fracturing and extension and asthenosphere upwelling and rift formation as the possible trigger for the volcanic eruptions in the region, which are distributed as linear features from west to east.

4.d. Magma sources and tectonic constraints

Figure 12 shows that the Tarim, Dunhuang-Alxa and NCC have similar volcanic zones along their northern margins or interiors, and their ages, petrology and tectonic setting are also broadly similar. Furthermore, all these zones seem to have originated from similar magmatic sources as a result of asthenospheric flow and mantle upwelling during the continuous assembly of continental blocks from earlier than 320 Ma to *c.* 250 Ma. These areas share the following common characteristics: post-orogenic belt overprinted by later volcanic eruptions (Fig. 12b) and tectonic activity during the continuous assembly of continents.

It is well established that numerous continental blocks converged towards the Siberian continent, as also confirmed by palaeomagnetic data. The sources of the associated magmatic activity may include asthenospheric flow, a mantle plume and delamination of the Tianshan – Inner Mongolia Orogenic Belt. The large-scale continental assembly would have been accompanied by asthenospheric flow, producing mantle upwelling. As noted above, delamination did not occur in this region when the large igneous province was formed in the Tarim Block. That the different volcanic suites, including basalt and gabbro to acid rhyolite, formed during the time interval 320–250 Ma suggests that the magmatic source was not from a mantle plume.

There was no subducting oceanic plate in this region during the period 280–230 Ma. Nevertheless, it is possible that an earlier subducted oceanic plate broke off beneath the continental margin, subsequently producing rifting and accompanying volcanic eruptions. However, there is no evidence to support this idea. Several unknowns related to this include: (1) the time gap before this subducted slab re-melted; and (2) whether the effect of the slab break-off was restricted to the formation of a rift in the crust or not. More likely the effects would also be found in the deeper lithosphere, although there are no post-collisional mantle-derived granites and no Permian uplift or mountain building. It therefore seems that the 290–280 Ma volcanic eruptions and rifting could only have resulted from continental convergence and assembly accompanied by the production of mantle-derived magmas, with no evidence for the break-off of an oceanic slab beneath the

https://doi.org/10.1017/S0016756815001077 Published online by Cambridge University Press

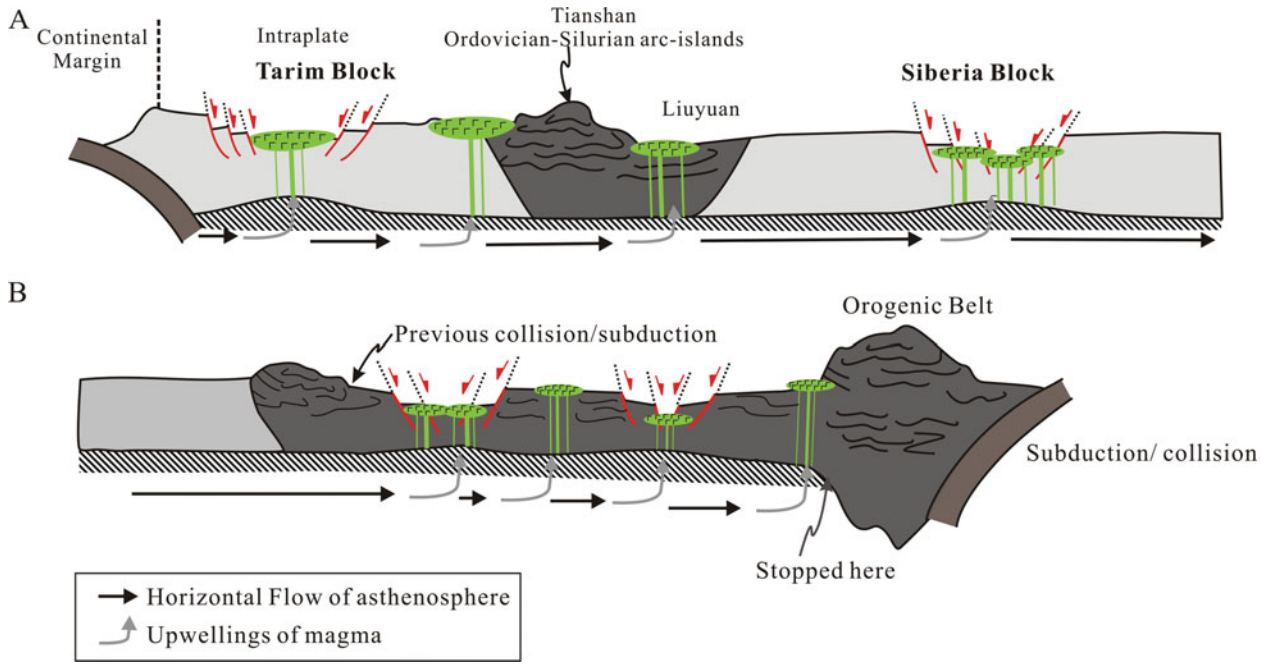

Figure 13. (Colour online) Plate tectonic model for the formation of intracontinental basaltic rocks during the assembly of continental blocks. (a) Basaltic rocks formed within the continental blocks and orogenic belt; and (b) basaltic rocks formed in the orogenic belt (post-orogen background). Horizontal flow of asthenosphere and upwelling of magma are also shown.

continental margin. The post-collisional tectonics show local rift features, but there is no evidence of regional extension. In fact, as well as the opening of the rift zone, there is no evidence for any detachment process.

Magma upwelling occurs from asthenospheric mantle, with the involvement of both depleted and enriched materials (Zhao *et al.* 2006; Jiang *et al.* 2007). Mantle plumes can produce variably enriched OIB-type lavas from highly enriched to less enriched (Safonova *et al.* 2009; Safonova & Santosh, 2014) depending on the height of the mantle column and local mantle metasomatism (Safonova *et al.* 2015). A diapir of asthenospheric magma may form in a rift system (Fig. 13). The formation of the volcanic rift belt was related to a new tectonic cycle that took place in the region after the main orogenic event; nevertheless, rifting took place when the continental area was still in an overall state of contraction (Fig. 13). Although the rifting (such as at Liuyuan) seems to have been related to a local extensional event in an overall contractional environment, such feature process can occur during or after the formation of orogenic belts, when convergence and the assembly of the continents or continental blocks occurs continuously. The asthenosphere would have changed its flow from horizontal under the continents to vertical (up or down) in soft or weak zones between blocks and orogenic belts (Fig. 13). Such flow patterns and upwelling of the mantle would have led to local intraplate or continental margin rifting (e.g. Schellart, 2008, 2010; Schellart & Moresi, 2013), overprinting the previous orogenic belt or active continental margin. In such a tectonic setting there is no uplift and no radial dyke swarms, therefore excluding the role of a mantle plume.

Formation of the rifts involves the reworking or re-extension of the continental margins during regional and continuous continental assembly. This rifting process was unrelated to subduction and to the delamination after lithospheric thickening following major collisional orogeny. The volcanic eruptions mostly occur along weak zones, or would even form the rift (fissuring) of a continent (Ziegler & Cloetingh, 2004), with both OIB and MORB features together with those of mafic and felsic end-members typical of a rift system.

5. Conclusions

The Liuyuan Volcanic Belt, which is part of the NE extension of the Tarim Block, shows features typical of a rift. Sandstones and claystones on both the southern and northern flanks of the rift zone show two types of sedimentary sources: 290–285 Ma volcanic tuffs and clastics; and 460–420 Ma granites and schists. The rift region is characterized by an older basement of 920–850 Ma belonging to the Dunhuang crystallines, together with younger 450–420 Ma granites and greenschists that were originally part of an Ordovician–Silurian island arc. The area was a continental realm prior to rifting, and there is no evidence along the rift zone of contemporaneous island-arc granites or other related intrusives with ages of 290–280 Ma. The pillow-lava basalts are covered by 277 Ma dacites and rhyolites, and are intruded by 280–270 Ma gabbro dykes. All these rocks were subjected to thrusting and folding during 230–227 Ma as a result of north–south contraction and intracontinental sinistral strike-slip deformation between the Xingxingxia Fault to the NW and the Altyn Tagh Fault to the SE. The

https://doi.org/10.1017/S0016756815001077 Published online by Cambridge University Press

nature of the sediments and volcanic eruptions in the rift, their compositions and their intrusive relationships all suggest a local rift system. During the formation of the rift there was no widespread extension; instead, the tectonic setting involved the continuous assembly of continental blocks that were moving from south to north, towards the Siberian continent. The formation and sources of the magmas during rifting were related to asthenospheric flow that accompanied the assembly of continental blocks during the period *c.* 300–250 Ma.

Acknowledgements. We greatly appreciate the constructive comments and suggestions from the editor of Geological Magazine, Dr Phil Leat, and two reviewers. This study was supported by the State Key Research Development Program of China (973, grant number 2011CB808901). Discussions with Professors B. F. Han, J. Y. Li and S. F. Liu improved this manuscript.

Supplementary material

To view supplementary material for this article, please visit http://dx.doi.org/10.1017/S0016756815001077.

References

Ao, S. J., Xiao, W. J., Han, C. M., Mao, Q. G. & Zhang, J. E. 2010. Geochronology and geochemistry of Early Permian mafic–ultramafic complexes in the Beishan area, Xinjiang, NW China: implications for late Paleozoic tectonic evolution of the southern Altaids. *Gondwana Research* **18**, 466–78.

Buiter, S. J. H. & Torsvik, T. H. 2014. A review of Wilson Cycle plate margins: a role for mantle plumes in continental break-up along sutures? *Gondwana Research* **26**, 627–53.

Cleven, N. R., Lin, S. F. & Xiao, W. J. 2015. The Hongliuhe fold-and-thrust belt: evidence of terminal collision and suture-reactivation after the Early Permian in the Beishan orogenic collage, Northwest China. *Gondwana Research* **27**, 796–810.

Cocks, L. R. M. & Torsvik, T. H. 2007. Siberia, the wandering northern terrane, and its hanging geography through the Palaeozoic. *Earth-Science Reviews* **82**, 29–74.

Geng, Y. S. & Zhou, X. W. 2011. Characteristics of geochemistry and zircon Hf isotope of the Early Neoproterozoic granite in Alax area, Inner Mongolia. *Acta Petrologica Sinica* **27**, 897–908 (in Chinese with English abstract).

Han, B. F., He, G. Q., Wang, X. C. & Guo, Z. J. 2011. Late Carboniferous collision between the Tarim and Kazakhstan–Yili terranes in the western segment of the South Tian Shan Orogen, Central Asia, and implications for the Northern Xinjiang, western China. *Earth-Science Reviews* **109**, 74–93.

Han, B. F., He, G. Q., Wang, S. G. & Hong, D. W. 1998. Post-collisional mantle-derived magmatism and vertical growth of the continental crust in North Xinjiang. *Geological Review* **44**, 396–406 (in Chinese with English abstract).

Jiang, C. Y., Cheng, S. L., Ye, S. F., Xia, M. Z., Jiang, H. B. & Dai, Y. C. 2006. Lithogeochemistry and petrogenesis of Zhongposhanbei mafic rock body, at Beishan region, Xinjiang. *Acta Petrologica Sinica* **22**, 115–26 (in Chinese with English abstract).

Jiang, C. Y., Xia, M. Z., Yu, X., Lu, D. X., Wei, W. & Ye, S. F. 2007. Liuyuan trachybasalt belt in the northeastern Tarim plate: products of asthenosphere mantle decompressional melting. *Acta Petrologica Sinica* **23**, 1765–78 (in Chinese with English abstract).

Kawachi, Y. & Pringle, I. J. 1988. Multiple rind structure in pillow lava as an indicator of shallow water. *Bulletin of Volcanology* **50**, 161–8.

Kennish, M. J. & Lutz, R. A. 1998. Morphology and distribution of lava flows on mid-ocean ridges: a review. *Earth-Science Reviews* **43**, 63–90.

Kröner, A., Kovach, V., Belousova, E., Hegner, E., Armstrong, R., Dolgopolova, A., Seltmann, R., Alexeiev, D. V., Hoffmann, J. E., Wong, J., Sun, M., Cai, K., Wang, T., Tong, Y., Wilde, S. A., Degtyarev, K. E. & Rytsk, E. 2014. Reassessment of continental growth during the accretionary history of the Central Asian Orogenic Belt. *Gondwana Research* **25**, 103–25.

Laurent-Charvet, S., Charvet, J., Shu, L. S. Ma, R. S. & Lu, H. F. 2002. Palaeozoic late collisional strike-slip deformations in Tianshan and Altay, eastern Xinjiang, NW China. *Terra Nova* **14**, 249–56.

Li, J. B., Kang, X., Wang, T., Li, W. P. & Tong, Y. 2006. Establishment of the Early Permian Hongliuhe Group in the Beishan area on the border region of Xinjiang and Gansu, China. *Geological Bulletin of China* **25**, 465–8 (in Chinese with English abstract).

Li, J. Y., He, G. Q., Xu, X., Li, H. Q., Sun, G. H., Yang, T. N., Gao, L. M. & Zhu, Z. X. 2006. Crustal tectonic framework of northern Xinjiang and adjacent regions and its formation. *Acta Geologica Sinica* **80**, 148–67 (in Chinese with English abstract).

Li, J. Y. & Xu, X. 2004. Major problems on geologic structures and metallogenesis of northern Xinjiang, NW China. *Xinjiang Geology* **22**, 119–24 (in Chinese with English abstract).

Liao, J. & Gerya, T. 2015. From continental rifting to seafloor spreading: insight from 3D thermo-mechanical modeling. *Gondwana Research* **28**, 1329–43.

Liu, C., Zhao, Z. H. & Guo, Z. J. 2006. Chronology and geochemistry of lamprophyre dykes from Beishan area, Gansu Province and implications for the crust–mantle interaction. *Acta Petrologica Sinica* **22**, 1294–306 (in Chinese with English abstract).

Liu, Y. S., Gao, S., Yuan, H. L., Zhao, L., Liu, X. M., Wang, X. C., Hu, Z. C. & Wang, L. S. 2004. U–Pb zircon ages and Nd, Sr, and Pb isotopes of lower crustal xenoliths from North China Craton: insights on evolution of lower continental crust. *Chemical Geology* **211**, 87–109.

Ludwig, K. R. 2005. *Isoplot: A Plotting and Regression Program for Radiogenic Isotope Data, Version 3.23*. Berkerly, CA, USA: Berkeley Geochronology Center.

Mao, Q. G., Xiao, W. J., Windley, B. F., Han, C. M., Qu, J. F., Ao, S. J., Zhang, J. E. & Guo, Q. Q. 2012. The Liuyuan complex in the Beishan, NW China: a Carboniferous–Permian ophiolitic fore-arc sliver in the southern Altaids. *Geological Magazine* **149**, 483–506.

Nance, R. D., Murphy, J. B. & Santosh, M. 2014. The supercontinent cycle: a retrospective essay. *Gondwana Research* **25**, 4–29.

Pan, J. H., Guo, Z. J. & Zhao, Z. H. 2008. Geochronology, geochemistry and tectonic implications of Permian basalts in Hongliuhe area on the border between Xinjiang and Gansu. *Acta Petrologica Sinica* **24**, 793–802 (in Chinese with English abstract).

Pirajno, F. 2015. Intracontinental anorogenic alkaline magmatism and carbonatites, associated mineral systems

and the mantle plume connection. *Gondwana Research* **27**, 1181–216.

PIRAJNO, F. & SANTOSH, M. 2015. Mantle plumes, supercontinents, intracontinental rifting and mineral systems. *Precambrian Research* **259**, 243–61.

QIN, K. Z., SU, B. X., LI, X. H., TANG, D. M., SAKYI, P. A., SUN, H., XIAO, Q. H. & LIU, P. P. 2011. SIMS zircon U–Pb geochronology and Sr–Nd isotopes of mafic–ultramafic intrusions in Eastern Tianshan and Beishan in correlation with flood basalts in Tarim Basin (NW China): constraints on a ca. 280 Mantle plume. *American Journal of Sciences* **311**, 237–60.

SACHAU, T. & KOEHN, D. 2010. Faulting of the lithosphere during extension and related rift-flank uplift: a numerical study. *International Journal of Earth Sciences (Geol Rundsch)* **99**, 1619–32.

SAFONOVA, I. YU, MARUYAMA, S. & LITASOV, K. 2015. Generation of hydrous-carbonated plumes in the mantle transition zone linked to tectonic erosion and subduction. *Tectonophysics* **662**, 454–71.

SAFONOVA, I. YU. & SANTOSH, M. 2014. Accretionary complexes in the Asia–Pacific region: Tracing archives of ocean plate stratigraphy and tracking mantle plumes. *Gondwana Research* **25**, 126–58.

SAFONOVA, I. YU., UTSUNOMIYA, A., KOJIMA, S., NAKAE, S., TOMURTOGOO, O., FILIPPOV, A. N. & KOIZUMI, K. 2009. Pacific superplume-related oceanic basalts hosted by accretionary complexes of Central Asia, Russian Far East and Japan. *Gondwana Research* **16**, 587–608.

SCHELLART, W. P. 2008. Kinematics and flow patterns in deep mantle and upper mantle subduction models: Influence of the mantle depth and slab to mantle viscosity ratio. *Geochemistry Geophysics Geosystems* **9**, Q03014, doi: 10.1029/2007GC001656.

SCHELLART, W. P. 2010. Mount Etna-Iblean volcanism caused by rollback-induced upper mantle upwelling around the Ionian slab edge: an alternative to the plume model. *Geology* **38**, 691–4.

SCHELLART, W. P. & MORESI, L. 2013. A new driving mechanism for backarc extension and backarc shortening through slab sinking induced toroidal and poloidal mantle flow: Results from dynamic subduction models with an overriding plate. *Journal of Geophysical Research: Solid-Earth* **118**, 3221–48.

Shaker Ardakani, A. R., ARVIN, M., OBERHÄNSLI, R., MOCEK, B. & MOEINZADEH, S. H. 2009. Morphology and petrogenesis of pillow lavas from the Ganj Ophiolitic Complex, southeastern Kerman, Iran. *Journal of Sciences, Islamic Republic of Iran* **20**, 139–51.

SIMONOV, V. A., MIKOLAICHUK, A. V., SAFONOVA, I. YU, KOTLYAROV, A. V. & KOVYAZIN, S. V. 2015. Late Paleozoic–Cenozoic intra-plate continental basaltic magmatism of the Tienshan–Junggar region in the SW Central Asian Orogenic Belt. *Gondwana Research* **27**, 1646–66.

SU, B. X., QIN, K. Z., SAKYI, P. A., LI, X. H., YANG, Y. H., SUN, H., TANG, D. M., LIU, P. P., XIAO, Q. H. & MALAVIARACHCHI, S. P. K. 2011*a*. U–Pb ages and Hf–O isotopes of zircons from Late Paleozoic mafic–ultramafic units in the southern Central Asian Orogenic Belt: Tectonic implications and evidence for an Early-Permian mantle plume. *Gondwana Research* **20**, 516–31.

SU, B. X., QIN, K. Z., SAKYI, P. A., LIU, P. P., TANG, D. M., MALAVIARACHCHI, S. P. K., XIAO, Q. H., SUN, H., DAI, Y. C. & HU, Y. 2011*b*. Geochemistry and geochronology of acidic rocks in the Beishan region, NW China: petrogenesis and tectonic implications. *Journal of Asian Earth Sciences* **41**, 31–43.

TIAN, Z. H., XIAO, W. J., SHAN, Y. H., WINDLEY, B. F., HAN, C. M., ZHANG, J. E. & SONG, D. F. 2013. Mega-fold interference patterns in the Beishan orogen (NW China) created by change in plate configuration during Permo–Triassic termination of the Altaids. *Journal of Structural Geology* **52**, 119–35.

TIAN, Z. H., XIAO, W. J., WINDLEY, B. F., LIN, L. N., HAN, C. M., ZHANG, J. E., WAN, B., AO, S. J., SONG, D. F. & FENG, J. Y. 2014. Structure, age, and tectonic development of the Huoshishan–Niujuanzi ophiolitic mélange, Beishan, southernmost Altaids. *Gondwana Research* **25**, 820–41.

WANG, Y., LI, J. Y. & SUN, G. H. 2008. Post-collision eastward extrusion and tectonic exhumation along the eastern Tianshan orogen, central Asia: constraints from dextral strike-slip motion and $^{40}Ar/^{39}Ar$ geochronological evidence. *Journal of Geology* **116**, 599–618.

WANG, Y., SANTOSH, M., LUO, Z. H. & HAO, J. H. 2015. Large igneous provinces linked to supercontinent assembly. *Journal of Geodynamics* **85**, 1–10.

WANG, Y., SUN, G. H. & LI, J. Y. 2010. U–Pb (SHRIMP) and $^{40}Ar/^{39}Ar$ geochronological constraints on the evolution of the Xingxingxia shear zone, NW China: a Triassic segment of the Altyn Tagh fault system. *Geological Society of America Bulletin* **122**, 487–505.

WANG, Y., ZHANG, X. M., ZHANG, J. F., WANG, E. C., LI, Q. & SUN, G. H. 2005. 40Ar–39Ar thermochronological evidence for formation and Mesozoic evolution of the northern–central segment of the Altyn Tagh Fault System in northern Tibetan Plateau. *Geological Society of America Bulletin* **117**, 1336–46.

XIAO, W. J., MAO, Q. G., WINDLEY, B. F., HAN, C. M., QU, J. F., ZHANG, J. E., AO, S. J., CLEVEN, N. R., LIN, S. F., SHAN, Y. H. & LI, J. L. 2010. Paleozoic multiple accretionary and collisional processes of the Beishan orogenic collage. *American Journal of Science* **310**, 1553–94.

XIAO, W. J. & SANTOSH, M. 2014. The western Central Asian Orogenic Belt: a window to accretionary orogenesis and continental growth. *Gondwana Research* **25**, 1429–44.

XIAO, W. J., SUN, M. & SANTOSH, M. 2015. Continental reconstruction and metallogeny of the Circum-Junggar areas and termination of the southern Central Asian Orogenic Belt. *Geoscience Frontiers* **6**, 137–40.

XIAO, W. J., WINDLEY, B. F., HUANG, B. C., HAN, C. M., YUAN, C., CHEN, H. L., SUN, M., SUN, S. & LI, J. L. 2009. End-Permian to mid-Triassic termination of the accretionary processes of the southern Altaids: implications for the geodynamic evolution, Phanerozoic continental growth, and metallogeny of Central Asia. *International Journal of Earth Science* **98**, 1189–217.

XU, X. Y., LI, R. S., CHEN, J. L., MA, Z. P., LI, Z. P., WANG, H. L., BAI, J. K. & TANG, Z. 2014. New constrains on the Paleozoic tectonic evolution of the northern Xinjiang area. *Acta Petrologica Sinica* **30**, 1521–34 (in Chinese with English abstract).

YAMAGISHI, H. 1985. Growth of pillow lobes: evidence from pillow lavas of Hokkaido, Japan and North Island New Zealand. *Geology* **13**, 499–502.

YANG, T. N., LI, J. Y., LIANG, M. J. & WANG, Y. 2015. Early Permian mantle–crust interaction in the south-central Altaids: high-temperature metamorphism, crustal partial melting, and mantle-derived magmatism. *Gondwana Research* **28**, 371–90.

YANG, T. N., WANG, Y., LI, J. Y. & SUN, G. H. 2007. Vertical and horizontal strain partitioning of the Central Tianshan (NW China): evidence from structures and

40Ar/39Ar geochronology. *Journal of Structural Geology* **29**, 1605–21.

ZHANG, C. L., ZOU, H. B., LI, H. K. & WANG, H. Y. 2013. Tectonic framework and evolution of the Tarim Block in NW China. *Gondwana Research* **23**, 1306–15.

ZHANG, C. L., ZOU, H. B., YAO, C. Y. & DONG, Y. G. 2014. Origin of Permian gabbroic intrusions in the southern margin of the Altai Orogenic belt: a possible link to the Permian Tarim mantle plume? *Lithos* **204**, 112–24.

ZHANG, W., WU, T. R., ZHENG, R. G., FENG, J. C., LUO, H. L., HE, Y. K. & XU, C. 2012. Post-collisional southeastern Beishan granites: geochemistry, geochronology, Sr–Nd–Hf isotopes and their implications for tectonic evolution. *Journal of Asian Earth Sciences* **58**, 51–63.

ZHANG, Y. Y., DOSTAL, J., ZHAO, Z. H., LIU, C. & GUO, Z. J. 2011. Geochronology, geochemistry and petrogenesis of mafic and ultramafic rocks from Southern Beishan area, NW China: Implications for crust–mantle interaction. *Gondwana Research* **20**, 816–30.

ZHAO, Z. H., GUO, Z. J., HAN, B. F., WANG, Y. & LIU, C. 2006. A comparative study on Permian basalt from eastern Xinjiang–Beishan area of Gansu Province, and its tectonic implications. *Acta Petrologica Sinica* **22**, 1279–93 (in Chinese with English abstract).

ZHAO, Z. H., GUO, Z. J., ZHANG, Z. C., SHI, H. Y. & TIAN, J. 2004. The geochemical characteristics and tectonic setting of the low Permian basalts in Hongliuhe area at the border between Xinjiang and Gansu provinces. *Geological Journal of China Universities* **10**, 534–45 (in Chinese with English abstract).

ZHOU, M. F., LESHER, C. M., YANG, Z. X., LI, J. W. & SUN, M. 2004. Geochemistry and petrogenesis of 270 Ma Ni-Cu-(PGE) sulfide-bearing mafic intrusions in the Huangshan district, Eastern Xinjiang, northwest China: implications for the tectonic evolution of the Central Asian orogenic belt. *Chemical Geology* **209**, 233–57.

ZIEGLER, P. A. 1992. Geodynamics of rifting. *Tectonophysics* **215**(1–2), 221–53.

ZIEGLER, P. A. & CLOETINGH, S. 2004. Dynamic processes controlling evolution of rifted basins. *Earth-Science Reviews* **64**, 1–50.

ZUO, G. C., LIU, Y. K. & LIU, C. Y. 2003. Framework and evolution of the tectonic structure in Beishan area across Gansu Province, Xinjiang Autonomous region and Inner Mongolia Autonomous region. *Acta Geologica Gansu* **12**, 1–15 (in Chinese with English abstract).

ZUO, G. C., ZHANG, S. L., HE, G. Q. & ZHANG, Y. 1991. Plate tectonic characteristics during the early Paleozoic in Beishan near the Sino-Mongolian border region, China. *Tectonophysics* **188**, 385–92.